ISSN 0256-4637
VOLUME 36 NUMBER 1 JANUARY-MARCH 2014

Journal of Pure and Applied

Ultrasonics

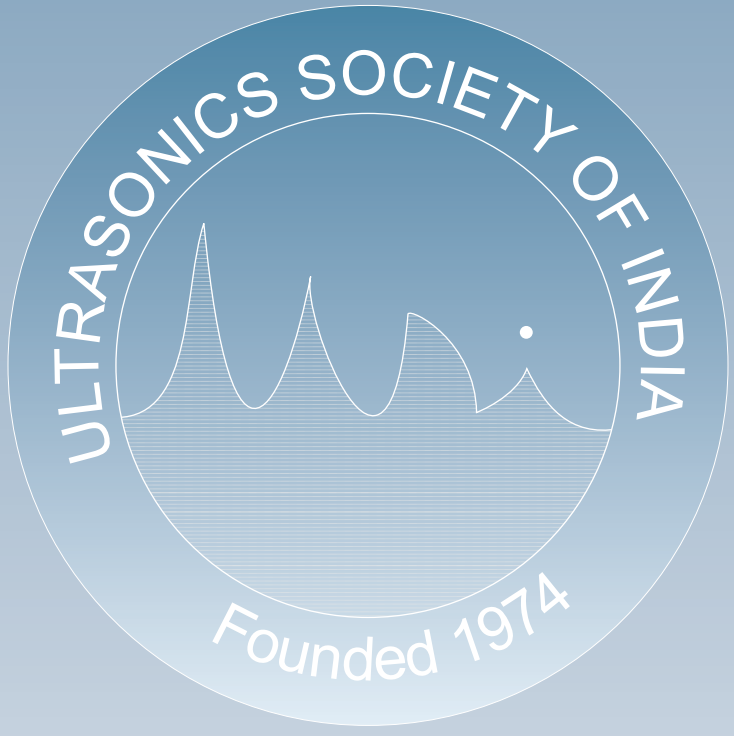

Website : www.ultrasonicsindia.org

A Publication of Ultrasonics Society of India

Ultrasonics Society of India

Ultrasonics Society of India established in 1974, is engaged in the promotion of research and diffusion of knowledge concerning the field of ultrasonics and allied areas.

Patrons : Dr. V.N. Bindal
Prof. E.S.R. Gopal

Executive Council :

President	Prof. Vikram Kumar
Vice-President	Dr.V.R. Singh
	Prof. R.R.Yadav
General Secretary	Dr. Mahavir Singh
Joint Secretary	Dr. Mukesh Chandra
Treasurer	Dr. Yudhisther Kumar Yadav
Publication Secretary	Dr. Devraj Singh
Members	Dr. S.K. Jain
	Dr. Janardan Singh
	Dr. J.N. Som
	Dr. K.P. Chaudhary
	Prof. S.S. Mathur
	Mr. I.S. Taak
	Dr. Sanjay Yadav
	Dr. S.K. Shrivastava
	Mr. V.K. Ojha
Co-opted member	Prof. Jacob Philip
	Prof. K. Balasubramaninam
	Mr. G. K. Arora
Past Patron	Prof. A.R. Verma
Past President	Dr. Krishan Lal

Membership of the Society is open to individuals without distinction of sex, race or nationality and to bodies who subscribe to the aims and objectives of the Society.

The membership fee is as follows :

Class of Membership	**Subscription (one time)**
Honorary Fellow	Nil
Life Fellow / Member	Rs 2500/-
Associate Member	Rs 1000/- (for 5 yrs.)
Corporate Member	Rs 20000/-
Life Fellow/ Member (Foreign)	US $ 150
Corporate Member (Foreign)	US $ 1000

Membership forms and the relevant information can be downloaded from the website or obtained from :

The General Secretary
Ultrasonics Society of India
CSIR-National Physical Laboratory
Dr. K.S. Krishnan Marg,
New Delhi-110012
E-mail : mahavir@nplindia.org

A Quarterly Publication of Ultrasonics Society of India

Journal of Pure and Applied

Ultrasonics

No. 1	Volume 36	January - March 2014

Chief Editor : Dr. S.K. Jain
e-mail : skjainnpl@yahoo.co.in, skjain@nplindia.org

Editorial Board :

Prof. S.S. Mathur	Ex. Professor, Indian Institute of Technology, New Delhi sartaj_mathur@rediffmail.com, sartajmathur@yahoo.co.in,
Dr. P. Palanichamy	IGCAR, Kalapakkam, Tamilnadu. ppc@igcar.gov.in
Prof. R.R. Yadav	Physics Department, Allahabad University, Allahabad (U.P.) rryadav1@rediffmail.com

Publication Committee :

Dr. Devraj Singh	Amity School of Engineering & Technology, New Delhi
Dr. Mahavir Singh	National Physical Laboratory, New Delhi
Dr. Sanjay Yadav	National Physical Laboratory, New Delhi
Dr.Yudhisther Kumar Yadav	National Physical Laboratory, New Delhi

SUBSCRIPTION (postage paid)

Single	Rs. 550/-	US$ 50/-
Annual	Rs. 2200/-	US$ 200/-
USI *members*	Free	

ADVERTISEMENT

The Journal offers opportunity of wide and effective publicity for the manufacturer, suppliers of ultrasonic equipment, device and materials and also for scientific instruments and components. Tariff is as follows :

Back Cover	Rs. 2500/-	US $ 100/-
Inside Cover	Rs. 1500/-	US $ 75/-
Full page	Rs. 1000/-	US $ 50/-
Half page	Rs. 600/-	US $ 30/-

Discount of 20% is admissible for 4 successive insertions.

The submission of papers and all other correspondence regarding the Journal may please be addressed to :

Publication Secretary
Journal of Pure and Applied Ultrasonics
C/o Ultrasonics Society of India
CSIR-National Physical Laboratory
Dr. K.S. Krishnan Road
New Delhi-110012
www.ultrasonicsindia.org

ISSN 0256–4637

Journal of Pure and Applied Ultrasonics

VOLUME 36 NUMBER 1 JANUARY–MARCH 2014

CONTENTS

Website : www.ultrasonicsindia.org

A Publication of — Ultrasonics Society of India

J. Pure Appl. Ultrason. 36 (2014) pp. 3-7

Implementation of bicepstral target classifier with support vector machines for noise sources in the ocean

Mohankumar K., Supriya M. H. and P. R. Saseendran Pillai

Department of Electronics,
Cochin University of Science and Technology, Cochin-682 022, Kerala
E-mail : supriadoe@gmail.com

Higher order spectral analysis is becoming one of the key areas in marine acoustic signal processing, especially for the classification and identification of noise generating mechanisms. This paper investigates the feasibility of a target classifier with bicepstral features. Bicepstral coefficients are extracted from the noise data waveform after framing and windowing operations. These features are then used to train a support vector machine classifier. Various kernels are analyzed for the performance measure. It is found that SVM with a radial basis function kernel could achieve a success rate of 80.5%. The kernel parameters were chosen after performing grid search and cross validation. The result indicates that the bicepstral features could be utilized efficiently to form feature sets that could greatly aid in the classification process.

Key words: Spectral analysis, bicepstral coefficients, vector machines. ocean noise

Introduction

The identification and classification of noise sources in the ocean has become a key task in modern underwater acoustic signal processing. The variability, diversity and abundance of such noise sources make this task a complex one. The classification problem, in general, can be decomposed into estimation of features or signatures of the source from a set of received signals by applying suitable feature extraction techniques followed by the application of a pattern recognition algorithm to the estimated source signatures, for final classification. So far, a number of techniques have been developed for extracting features from the emanated sound[1-4], and majority of them centers around the classical power spectral analysis. Based on spectral analysis, a number of improved methods were also proposed, including the cepstrum and wavelet analysis and has gained considerable attention from the research community.

However, being a linear method, power spectral analysis cannot fully characterize the non-linear signals and noise generating mechanisms. It also does not preserve the phase information contained in the signal. This, coupled with the complex nature of the radiated noise signals, which actually are composites of diverse sources, some of which are totally stochastic and nonlinear, calls for the use of non-Gaussian and non-linear feature extraction techniques. This could reveal many more hidden signatures that can lead to efficient classification of the noise generating mechanisms.

For instance, it is shown that detection and acquisition of stable and reliable nonlinear features become practically feasible by nonlinear analysis of the time series of radiated sounds from ships[5]. To capture the nonlinear characteristics, the acoustical noises are analyzed in subspaces of intrinsic mode functions attained via the ensemble empirical mode decomposition. In yet another work[6], Yang et al. confirmed the existence of nonlinearity in underwater signals, achieving promising results based on the concept of fractals, proving the usefulness and effectiveness of the nonlinear feature.

Methods based on higher order signal processing have also proven to be effective in detecting and characterizing non-Gaussianity and nonlinearity. Hinich has analyzed noise radiations from ships[7] using bispectrum. Richardson and Hodgkiss[8] estimated the bispectra of data taken from freely drifting swallow float and has demonstrated how the bispectrum estimate can be used to detect non-Gaussianity, nonlinearity and harmonic couplings.

The bispectrum has also proven to be useful in a number of applications in different domains, varying from fault detection to the analysis of power generation systems. For instance, bicoherence analysis[9] has been used to characterize the nonlinear effects of jet noise propagation.

Acoustic emission in steel pipes has been studied in literature[10] using bispectrum to analyze the results of a deformation test.

Preliminaries

Moments and cumulants

For a given set of n real random variables $\{x_1,x_2,..x_n\}$ their joint moments of order $r = k_1 + k_2 + ...+k_n$ is given by Nikias and Raghuveer[11].

$$m_{k_1....k_n} = E\{x_1^{k_1} x_2^{k_2} ...x_n^{k_n}\}$$

ie.,

$$m_{k_1....k_n} = (-j)^r \left.\frac{\partial^r \phi(\omega_1^{k_1},\omega_2^{k_2},...,\omega_n^{k_n})}{\partial(\omega_1^{k_1},\omega_2^{k_2},...,\omega_n^{k_n})}\right|_{\omega_1=\omega_2...=\omega_n=0}$$

where $\phi(\omega_1^{k_1},\omega_2^{k_2},...,\omega_n^{k_n})$ is their joint characteristic function. Specifically, for a real stationary random process, the moments can be estimated by taking the expectation over the process multiplied by (n-1) lagged versions of itself.

The joint cumulants of order r of the same set of random variables are defined as

$$c_{k_1....k_n} = (-j)^r \left.\frac{\partial^r \ln\phi(\omega_1^{k_1},\omega_2^{k_2},...,\omega_n^{k_n})}{\partial(\omega_1^{k_1},\omega_2^{k_2},...,\omega_n^{k_n})}\right|_{\omega_1=\omega_2..=\omega_n=0}$$

It can be seen that cumulants are very closely related to moments, except for the use of natural logarithm of the characteristic function, instead of the characteristic function itself.

Cumulant spectra

The nth order cumulants spectrum $c_n(\omega_1,\omega_2,...\omega_n)$ of a stationary process {X(k)} is defined as the Fourier Transform of its n[th] order cumulants sequence[11].
That is,

$$C_n(\omega_1,\omega_2,...\omega_{n-1}) = \sum_{\tau_1=-\infty}^{\infty} ... \sum_{\tau_{n-1}=-\infty}^{\infty} c_n(\tau_1,...,\tau_{n-1}) \exp\{-j(\omega_1\tau_1 + ... + \omega_{n-1}\tau_{n-1})\} \quad (1)$$

The first member of the polyspectrum family is the fourier transform of the second order cumulant (n = 2) or the autocorrelation sequence. ie.,

$$C_2(\omega_1) = \sum_{\tau=-\infty}^{\infty} c_2(\tau_1)\exp(-j\omega_1\tau_1) \quad (2a)$$

$$= E\{X(f)X^*(f)\} \quad (2b)$$

where $c_2(\tau_1)$is the second-order cumulant.

Similar to the power spectrum, the third order spectrum or the bispectrum is defined as

$$C_3(\omega_1,\omega_2) = \sum_{\tau_1=-\infty}^{\infty}\sum_{\tau_2=-\infty}^{\infty} c_3(\tau_1,\tau_2)\exp\{-j(\omega_1\tau_1+\omega_2\tau_2)\} E\{X(f_1)X(f_2)X^*(f_1+f_2)\} \quad (3)$$

where $c_3(\tau_1,\tau_2)$ is the auto-bicorrelation or the third order cumulant sequence.

Polycepstra

The poly cepstrum can be obtained similarly to the (power) cepstrum by taking the logarithm of the corresponding polyspectrum and inverse transforming the log-spectrum. Similar to the polyspectrum, the poly-cepstrum is called power cepstrum for n = 2, bicepstrum for n = 3 and tricepstrum for n = 4.

The definition of the cepstrum in terms of higher order cumulants enables us to retrieve the cepstrum of the source wavelet analytically, when the reflectivity does not consist of a train of spikes. Since the bispectrum and the trispectrum conserve the phase characteristics of the wavelet, it is evident that the cepstrum derived from these polyspectra will also conserve phase information.

Bicepstral estimation

Bicepstrum is defined as the inverse 2D z-transform of log bispectrum[6] *i.e.*,

$$b_h(n,m) = Z_2^{-1}(\log(C_3(\omega_1,\omega_2)) \quad (4)$$

Defining $\log(C_3(\omega_1,\omega_2))$ as $B_h(\omega_1,\omega_2)$ and taking partial differentiation,

$$\frac{\partial B_h(\omega_1,\omega_2)}{\partial\omega_1} = \frac{1}{C_3(\omega_1,\omega_2)}\frac{\partial C_3(\omega_1,\omega_2)}{\partial\omega_1}$$

Re-arranging,

$$C_3(\omega_1,\omega_2)\frac{\partial B_h(\omega_1,\omega_2)}{\partial\omega_1}\omega_1 = \frac{\partial C_3(\omega_1,\omega_2)}{\partial\omega_1}\omega_1 \quad (5)$$

From Eq. (5) it can be shown that [6], the bicepstrum $b_h(n,m)$ and the third order moment sequence $m_3(n,m)$ can be related by the linear convolution formula

$$-n.m_3(n,m) = m_3(n,m)*(-mb_h(n,m)) \quad (6)$$

A method for computing the cepstrum coefficients that does not require phase unwrapping can be derived from Eq. (6) based on two-dimensional Fast Fourier Transform operations as:

$$n \cdot b_h(n,m) = F_2^{-1}\left\{\frac{F_2\,(n \cdot m_3(n,m))}{F_2\,(m_3(n,m))}\right\} \quad (7)$$

where F (*) represents the 2-D Fourier transform.

Thus, the steps for bicepstral estimation can be summarized as:

a) Segment the waveform data into R records of N samples each.
b) Mean adjust each record by subtracting the mean
c) Estimate the third order moment sequence for each record using the formula

$$m_3(n,m) = \frac{1}{N}\sum x(k)x(k+n)x(k+m)$$

and compute the average moment sequence.

d) Compute the bicepstrum coefficients using the 2D Fourier transform using Eq. (7).

Support Vector Machines (SVM)

Support vector machines (SVM) are a group of supervised learning methods that can be applied to classification or regression[12]. SVMs, in its original implementation function as a binary classifier. Its popularity has grown ever since in various areas of research in pattern recognition and has been extended to multiclass separation problems.

The theory behind SVM relies on the fact that it is possible to transform the data into a space where the classes are linearly separable with dimensionality at least equal to the Vapnik-Chervonenkis (VC) dimension of the data[12]. In that space, an SVM will find the data patterns that are closest to the border between the classes and these patterns are called the Support Vectors, since they are the support for choosing the optimal hyperplane that separates the classes. An SVM classifier will then choose the hyperplane that is equidistant from the patterns of different classes.

Consider a set of linear separable training samples x_i and corresponding labels y_i, where, $1 \le i \le L$, $x \in \Re^d$ and $y \in$, {1,1}. In its general form, the supervised learning can be treated as constructing an optimal classifier function f that maps x_i to y_i. The general form of a linear classification function can be represented as

$$f(x) = w.\,x + b \quad (8)$$

which corresponds to a separating hyperplane:

$w.\,x + b = 0$

subject to the constraint $y_i\,(w.x_i + b) \ge 1$

By introducing the Lagrange multipliers, the solution to this can be expressed as $w = \sum_i \alpha_i y_i x_i$ where α_i are the Lagrange multipliers. Thus,

$$f(x) = sign(\sum_i \alpha_i y_i x_i \cdot x + b) \quad (9)$$

When data is not linearly separable, a non-linear mapping function ϕ may be used so that Eq. (9) may be re written as

$$f(x) = w.\phi(x) + b \quad (10)$$

By introducing slack variables and penalty factors, Eq. (10) may be modified as

$$f(x) = sign(\sum_i a_i y_i k(x_i \cdot x) + b) \quad (11)$$

where, $k(x_i,x)$ is a Kernel function. There are a very wide variety of possible Kernel functions (although they must satisfy Mercer's theorem), including linear, polynomials and radial basis functions (RBFs).

Linear : $k(x_i,x) = x_i^T \cdot x$

Polynomial : $k(x_i,x) = (x_i^T \cdot x + 1)^d$

RBF : $k(x_i,x) = e^{-\|x-x_i\|^2/(2\sigma^2)}$

Methodology

The preprocessed noise data waveforms were segmented to form frames of equal length. The individual frames are windowed to minimize the signal discontinuities at the boundaries of each frame caused by the Gibb's phenomenon. If the window is defined as W[n], then the windowed signal $X_w[n]$ is given by

$X[n] = X[n] \otimes W[n]$, where $0 \le n \le N_s - 1$

The number of samples in each frame N_s, was chosen to be 10240 samples, which corresponds to the data for the duration approximately one second. The bicepstral coefficients were computed from the windowed frames by applying Eq. (7).

The features obtained are then used to train a SVM, with suitable Kernel and kernel related parameters. For any kernels, there will be some parameters that would determine the properties and efficiency of the classifier. For instance, there are two parameters for an RBF kernel, namely C and λ. The optimal values for these parameters are not known beforehand and consequently some kind of model selection (parameter search) must be done to identify them, thereby ensuring best possible performance of the classifier.

Cross-validation and Grid-search is an efficient and simple strategy for identifying such optimal values for the kernel parameters. The basic idea is to separate the data set into two parts, of which one is considered unknown. In a v-fold cross-validation, we first divide the training set into v subsets of equal size. Sequentially

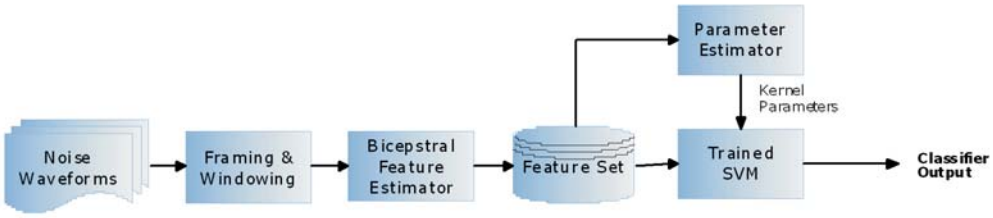

Fig. 1–Feature extraction and classification

one subset is tested using the classifier trained on the remaining (v - 1) subsets. Thus, each instance of the whole training set is predicted once so the cross-validation accuracy is the percentage of data which are correctly classified. Generally a grid-search on C and γ is employed using cross-validation, in such a way that various pairs of C and γ values are tried and the pair with the best cross-validation accuracy is picked. The values of the parameters are generally chosen from an exponentially growing sequence. The whole procedure of feature extraction and classification is illustrated in Fig. 1.

Results and Discussion

The noise data waveforms were sliced into records of equal length and the bicepstral coefficients for each record were computed. As an illustration, Figures 1(a) and 1(b) show the contour and mesh plots of a record of a boat, while Figs 2(a) and 2(b) show the contour and mesh plot of another target, which is a ship.

Three SVMs where designed with Linear, Polynomial and RBF kernels and trained with the extracted features. Kernel Parameters were estimated with Grid search Method. The noise data used for evaluating the proposed classifier mainly comprises of man-made and biological

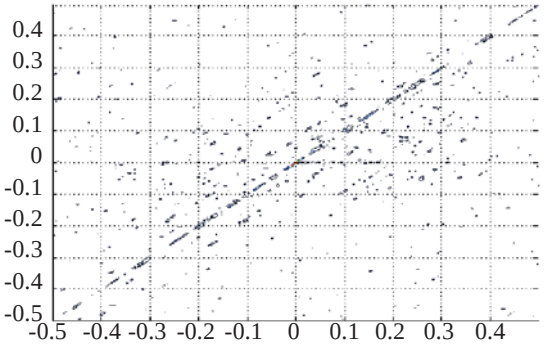

Fig. 1–(a) Contour plot of 256 × 256 bicepstral coefficients of one record of boat noise

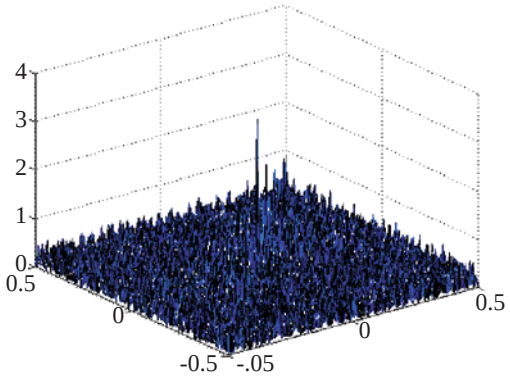

Fig. 1–(b) Mesh plot of 256 × 256 bicepstral coefficients of one record of boat noise

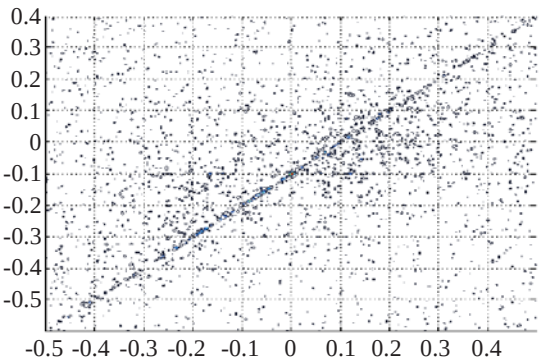

Fig. 2–(a) Contour plot of 256 × 256 bicepstral coefficients of one record of ship noise

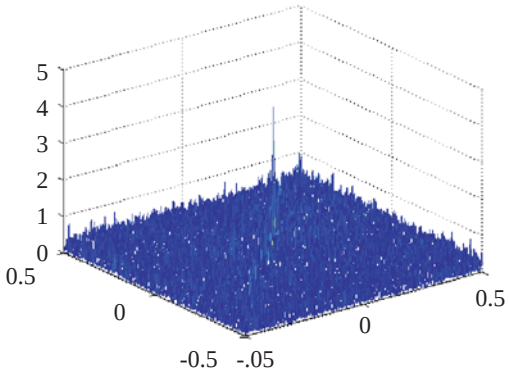

Fig. 2–(b) Mesh plot of 256 × 256 bicepstral coefficients of one record of ship noise

noises collected using hired vessels and also during the cruises off Cochin and Mangalore.

For the purpose of validating the performance of the classifiers, 400 records collected from 20 different targets were considered. SVM classifiers with Linear and Polynomial Kernels could achieve cumulative success rate of 78% and 79.5%. However, the prototype system with an RBF Kernel could correctly classify 322 records out of the 400 records, leading to a cumulative success rate of 80.5%. Thus, the higher order signal analysis techniques are found to reveal certain hidden characteristics of noise sources, and it could be augmented with classical methods to obtain improved success rates.

Conclusion

An SVM algorithm based classifier was developed and the performance was analyzed for the classification of manmade noise sources in the ocean. Target features were extracted using bicepstral analysis. It is found that, the proposed scheme could fairly classify the noise sources in the ocean with acceptable success rates using an RBF kernel.

Acknowledgments

The authors gratefully acknowledge the Department of Electronics, Cochin University of Science and Technology, for extending all the facilities for carrying out this work.

References

1 Deaett M. A., "Signature modeling for acoustic trainer synthesis," *IEEE J. Ocean. Eng*., 12 (1987) 143-147.

2 Arveson P. T. and Vendittis D. J., "Radiated noise characteristics of a modern cargo ship," *J. Acoust. Soc. Am*., 107 (2000) 118-129.

3 Wales C. and Heitmeyer R. M., "An ensemble source spectra model for merchant ship-radiated noise," *J. Acoust. Soc. Am*., 111 (2002) 1211-1231.

4 Boser B. E., Guyon I. M. and Vapnik V. N., "A training algorithm for optimal margin classifiers," Workshop on Computational Learning Theory, 5th Annual, Pittsburgh, Pennsylvania, United States, ACM Press, (1992).

5 Bao F., Li C., Wang X., Wang Q. and Du S., "Ship classification using nonlinear features of radiated sound: An approach based on empirical mode decomposition", *J. Acoust. Soc. Am*., 128(1) (2010) 206-14.

6 Yang S., Li Z. and Wang X., "Ship recognition via its radiated sound: the fractal based approaches.", *J. Acoust. Soc. Am*., 112(1) (2002) 172-7.

7 Hinich M. J., Marandino D. and Sullivan E. J., "Bispectrum of ship- radiated noise," *J. Acoust. Soc. Am.*, 85 (1989) 1512-1517.

8 Richardson A. M. and Hodgkiss W. S., "Bispectral analysis of under- water acoustic data," *J. Acoust. Soc. Amer*., 96(2) (1994) 828-836.

9 Gee, Kent L., Atchley, Anthony A., Falco, Lauren E., Shepherd, Micah R., Ukeiley, Lawrence S., Jansen, Bernard J., Seiner and John M., "Bicoherence analysis of model-scale jet noise", *J. Acoust. Soc. Amer.*, 128(5) (2010).

10 Juan José González de la Rosa, Rosa Piotrkowski, and José Evaristo Ruzzante, "Higher Order Statistics and Independent Component Analysis for Spectral Characterization of Acoustic Emission Signals in Steel Pipes", *IEEE Trans. on Instrumentation and Measurement*, 56(6) (2007).

11 Nikias C. and Raghuveer M., 'Bispectrum estimation: A digital signal processing framework', *Proc. IEEE*, 75 (1987) 869-889.

12 Cortes C. and Vapnik V., Support-vector network. "Machine Learning", (1995) 273-297.

J. Pure Appl. Ultrason. 36 (2014) pp. 8-12

Study of ultrasonic attenuation using two state model

V.K. Pundhir

Sagar Institute of Research & Technology Excellence, Ayodhya Bypass Road
Bhopal 462 041 (M.P.) India
E-mail : vivekpundhir@yahoo.com

Acoustical measurements in liquid metals have been primarily concerned with the direct measurement of ultrasonic velocity and attenuation in order to obtain information on their structures and thus contributing our knowledge of the liquid state. Ultrasonic attenuation measurement in particular provides means of distinguishing the non-atomic behavior or otherwise of simple liquid metals, which are notably different from the non-metallic liquids in that the major contribution to the attenuation is due to the thermal conductivity loss. A theoretical model has been developed on the lines of the two-state model applicable for associated liquids. This model renders satisfactory results for the excess ultrasonic attenuation in the liquid metals.

Keywords: Liquid metals, ultrasonic attenuation, ultrasonic relaxation, transport properties

Introduction

Theory of ultrasonic attenuation

The ultrasonic attenuation in a substance is observed using the process of sending the waves (longitudinal / transverse) to the specimen and then studying the output. The block diagram represents the complete process.

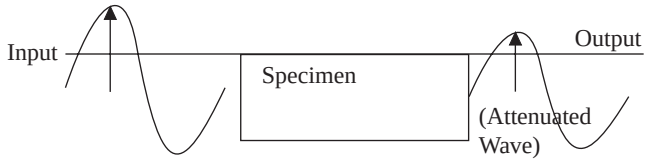

Fig. 1–Block diagram of the ultrasonic attenuation process

Analysis of the attenuated wave gives information of the physical processes responsible for the attenuation of acoustical energy by the specimen.

The classical attenuation (α_{cl}) coefficient is given by the addition of the viscous (α_S) and the thermal (α_T) attenuation coefficients, such that

$$\alpha_{cl} = \alpha_S + \alpha_T \tag{1}$$

$$\alpha_{cl} = \frac{2\pi^2}{\rho_l c_l^3}\left(\frac{4}{3}\eta_s + \frac{c_l^2 \alpha_p^2 K_T T}{c_p^2 J}\right) f^2 \tag{2}$$

where, ρ_l = density of the liquid metal, c_l = the ultrasonic velocity of the longitudinal wave in [100] direction, η_s = shear viscosity, α_p = the expansion coefficient, K_T = thermal conductivity, c_p = the specific heat at constant pressure, f = ultrasonic frequency, J = joules constant.

Liquid metals show the existence of excess ultrasonic attenuation over the classical value.

The excess attenuation coefficient (α_B) is formally attributed to a bulk viscosity η_B defined by

$$\alpha_B = \alpha - \alpha_{cl} \tag{3}$$

$$\alpha_B = \left(\frac{2\pi^2}{\rho_l c_l^3}\right)\eta_B f^2$$

$$\frac{\alpha_B}{f^2} = \left(\frac{2\pi^2}{\rho_l c_l^3}\right)\eta_B \tag{4}$$

where α is the experimental value of the ultrasonic attenuation coefficient.

There are no viscometers available which measures bulk viscosity of a liquid metal. The measurement of ultrasonic attenuation plays a unique role in the study of bulk viscosity. There are many different mechanisms of bulk viscosity. For example, in the non associated liquids, rotational isomeric and vibrational relaxation are the

major causes of the bulk viscosity, whereas in the associated liquids, structural relaxation effects are most important. In what follows we will be concerned only with the structural contribution to the bulk viscosity.

Two-state model and structural relaxation theory

To describe the structural relaxation processes in monatomic fluids, a simplest two-state model is assumed[1-2]. According to this model two structures are present near the melting point having different coordination numbers, corresponding, respectively, to the order of packing in the solid state and to a hard sphere like packing in the liquid state. State I is the one having lower free energy and higher packing fraction and corresponds to the solid phase on freezing. State II has higher free energy and lower packing fraction and corresponds to the liquid phase above the melting point.

At a particular temperature and pressure a certain fraction of the number of atoms would be in state I, and the remaining fraction would be in another state. When sound wave passes through the medium, the equilibrium distribution of the number of atoms in the two states is perturbed. The energy required by an atom to jump from one state to another is known as the activation energy and is equal to the difference in the free energy ΔF of the two states. The equilibrium would be established again after a lapse of a finite time. This finite time is known as the relaxation time for the process and can be represented by τ.

Evaluation of $(\Delta V/V)$, βr & τ

Various compressibility

Under the structural relaxation process, the liquid possesses a compressibility β_o, which is constituted by two components as follows:

$$\beta_\circ = \beta_r + \beta_\infty \tag{5}$$

where β_o, β_r and β_∞ are total, relaxation and instantaneous compressibility

Ultrasonic energy is attenuated in the liquid metals and the ultrasonic attenuation coefficient α_B (for $\omega\tau$<<1) due to structural relaxation, can be written as:

$$_B \quad \frac{2\ ^2}{c_l} \quad \frac{_r}{_0} \quad f^2$$

Or,
$$\alpha_B = \left(\frac{2\pi^2}{c_l}\right)\left(\frac{\beta_r \tau}{\beta_0}\right) f^2 \tag{6}$$

In order to obtain the expression for β_r and τ, we use a relaxation treatment for the configurational component of the compression. The simple assumption of a relaxation process with the two energy states mentioned above is necessary in this case. Using a relaxational treatment discussed[3-4], we obtain the following expression for β_r:

$$\beta_r = \frac{V\left(\frac{\Delta V}{V}\right)^2}{2RT\left[1+\cosh\left(\frac{\Delta F}{RT}\right)\right]} \tag{7}$$

here V is the molar volume of the liquid metal and $\Delta V/V$ is the relative change in the volume, under structural relaxation for the liquid metal concerned. $\Delta V/V$ essentially represents the difference in the packing fractions of state I (solid phase) and state II (liquid phase), above the melting points.

The relaxation time τ

The relaxation time τ can be obtained using Erying's theory of reaction rates[3,5], which gives the following expression for τ:

$$\tau = \frac{V\eta_s}{RT\left[1+\exp\left(\frac{\Delta F}{RT}\right)\right]} \tag{8}$$

In order to obtain the values of α_B, the attenuation coefficient due to structural relaxation using Eq. (6), we need the values of β_o and β_r and τ, which can be obtained independently as,

$$\beta_o = \frac{1}{\left(c_1^2\rho_1\right)} \tag{9}$$

here ρ_1 , density of the liquid metal and c_1 is the ultrasonic wave velocity in the concerned liquid metal. Similarly, β_∞ can be calculated from the following relation;

$$\beta_\infty = \frac{1}{\left(c_s^2\rho_s\right)} \tag{10}$$

here c_S is the longitudinal ultrasonic wave velocity in the solid phase of the metal concerned and ρ_S is the density of the solid metal.

Determination of packing fraction, ΔV/V

The packing fractions of the solid phase (state I) are very well known for all the metals. Alkali metals have the bcc structure with a packing fraction of 0.68. Cadmium has a hexagonal close-packed structure with packing fraction 0.74. Lead has fcc structure with packing fraction of 0.74.

Bismuth and tin have complex structures. While bismuth has only one form (rhombohedral) with $\xi \sim 0.74$, tin has two modifications - (a) gray tin (diamond structure) with $\xi = 0.34$, and (b) white tin which has a much greater packing fraction than that of gray tin. Gray tin is stable at low temperature, whereas white tin is stable at high temperatures and also near the melting point. Let us now examine the situation in the liquid phase. A hard sphere packing fraction defined as:

$$\xi = \frac{1}{6}\pi n\sigma^3$$

here ξ is the packing fraction of the total volume occupied by the spheres of diameter σ and n is the number of density of atoms, which plays an important role in comparing the results of various models proposed for the inter-particle potential functions in the liquid metals. According to Ashcroft and Lekner (1966)[6] it is possible to obtain a good representation of the liquid structure by choosing a packing fraction between 0.40 and 0.50. In fact most of the experimental results in liquid metals can be explained with a hard sphere packing fraction $\xi \sim 0.45$. To be specific, Stroud and Ashcroft (1972)[7] obtained theoretically the melting temperature of sodium as a function of pressure with hard sphere packing fraction of 0.42. Their results are in agreement with the experimental data.

We have taken $\Delta V/V = 0.27$ for liquid sodium, potassium, rubidium and cesium. This essentially represents the relative change of the molar volume when these metals change their structure from bcc type (ξ= 0.68) to the hard sphere liquid phase ($\xi = 0.41$). We take $\Delta V/V = 0.29$ for liquid lead, cadmium and bismuth. Here the solid phase has the packing fraction $\xi = 0.74$ and the liquid phase, $\xi = 0.45$. Tin is a peculiar case because in the solid phase $0.34 \leq \xi < 0.74$. Its structure is made up of two interpenetrating fcc lattices. Probably before freezing the fcc lattices get detached from each other and behave as a closed - packed lattice with $\xi = 0.74$, because we have tried this particular metal with $\Delta V/V = 0.29$ as for other close-packed metals like lead, cadmium and bismuth and surprisingly our results compare fairly well with the experimental values. Generally it is seen that the basic structure is the same in the liquid state of many metals, which have very different structure as solids. The conclusion suggested is that the close-packed cubic structure, which is the simplest of all known structures, is the dominating basic structure for liquid metals. This possibly is the reason that our $\Delta V/V$ values cluster around 0.29 which is the difference between the packing fraction of the close-packed state with $\xi = 0.74$ in solid phase and $\xi = 0.45$, the packing fraction of the hard sphere liquid.

The value of $\Delta V/V$ for the Hg, Zn and Ga are estimated on the basis of the structure of the crystal. Here Hg is rhombic hence $\Delta V/V = 0.29$, Zn is hcp hence $\Delta V/V = 0.30$ and Ga has an orthorhombic (complex) structure, so we estimate 0.29. As for other metals $\Delta V/V$ are taken from the literature[8,9].

Calculation of the Ultrasonic Attenuation in the Liquid Metals

Study of the temperature dependence of the ultrasonic attenuation in sodium, potassium, rubidium, cesium and bismuth[10,11] has shown the bulk viscosity decreases with increasing temperature and that relationship between (η_B/η_S) and ΔS (the entropy of melting) observed in liquid metals put them at par with associated liquids in certain physical phenomena. The structural relaxation processes have been investigated in several hydrogen-bonded (associated) liquids and the results so obtained are extremely in agreement with experimental results. Awasthi and Pundhir (2005)[12] have calculated recently the ultrasonic attenuation in the liquid zinc, gallium and mercury.

At first, we have calculated the values of β_0 and β_∞, and then calculated β_r and ΔF by Eq. (7) and τ has been calculated by using the eq. (8). The values of η_s are taken from literature[8, 9]. In order to calculate β_r and β_∞ the values of c_l, ρ_l ,c_s, and ρ_s for the Hg , Zn and Ga are taken from the literature[13,8,9,14-16]. In order to calculate β_∞, we have taken the values of c_s and ρ_s sodium, cadmium, tin, lead and bismuth from ref.[17], for potassium from ref.[18], for cesium from ref.[19] and for rubidium from ref.[20].

We have calculated the value of ultrasonic attenuation coefficient of 11 liquid metals (Table 3) by classical

attenuation coefficient α_{cl} / f^2 by using the Eq. (2) and by the theory of the two-state model [Eq. (6)] The experimental values also listed in Table 3 are taken from the literature[21, 9, 22]. The concept, theory and the relevant data are taken from March (1990)[23]. Tables 1and 2 show the required data of the relevant parameters used to evaluate the excess ultrasonic attenuation in the liquid metal.

Table 1–Listing of the values of β_o, β_r and β_∞

S. No.	Liquid Metal	β_o ($\times 10^{-12}$)	β_∞ ($\times 10^{-12}$)	β_r ($\times 10^{-12}$)
1	Na	16.90	10.73	06.170
2	K	33.98	19.00	14.980
3	Zn	01.856	0.6613	01.245
4	Ga	01.992	02.254	-0.260
5	Rb	42.70	21.62	21.080
6	Cd	02.65	01.154	01.496
7	Sn	02.36	01.27	01.090
8	Cs	58.12	23.12	35.000
9	Hg	03.419	02.332	01.087
10	Pb	02.96	01.88	01.076
11	Bi	03.67	01.99	01.679

Here fourth column shows the excess value (difference of experimental and classical value) obtained by Eq. (4), while the fifth column shows the excess ultrasonic attenuation obtained by using the two-state thermodynamical theoretical model (by Eq. 6).

Results and Discussion

The values of ultrasonic attenuation in various liquid metals are listed in the Table 3. As is obvious from Table 3 our values of α_B/f^2 calculated on the assumption of a two-state thermodynamical model compare fairly well with the experimental data. Our estimated values of α_B / f^2 are also listed in Table 3.

The relaxation time obtained for these liquid metals is of the order of 10^{-12} s, which is typically the value for many associated liquids as well are listed in Table 2.

The calculated values of ΔF for most of the liquid metals compare fairly well with the values of ΔF, obtained by Wilson[23] on fitting the experimentally obtained values of the shear viscosity for various liquid metals in the empirical relation of the form:

$\eta_S = A \exp(\Delta F/RT)$.

This linear relationship between the ΔF values obtained due to structural relaxation with the one responsible for shear viscosity suggests a close relationship between η_B and η_S. The temperature - independent behaviour of η_B / η_S can be explained by similar temperature dependence of η_B and η_S which is confirmed by the nature for both kinds of viscosities.

Table 2–The value of T, c_l, ρ_l, $\Delta V/V$, ρF, η_s and τ are listed with their proper unit

Liquid Metal	T (K)	c_l (10^5 cm/s)	ρ_l (g/cm^3)	$\Delta V/V$	ΔF (kcal mol^{-1})	η_s (10^{-2}poise)	τ (10^{-12}s)
Na	373	2.526	0.9269	0.27	01.47	0.705	0.68
K	348	1.890	0.8237	0.27	01.21	0.503	01.22
Zn	723	2.790	06.920	0.30	3.180	3.027	0.47
Ga	303	2.870	06.095	0.29	---	1.950	---
Rb	316	1.260	01.475	0.27	01.06	0.670	02.29
Cd	633	2.166	8.0310	0.29	3.20	1.440	0.28
Sn	513	2.464	6.9690	0.29	03.41	2.100	0.28
Cs	308	0.969	1.8400	0.27	01.07	0.690	2.87
Hg	298	1.470	13.534	0.29	2.235	1.610	0.21
Pb	613	1.776	10.6800	0.29	04.03	2.560	0.34
Bi	553	1.645	10.0600	0.29	03.31	1.830	0.39

On observing Table 3, we find that the excess ultrasonic attenuation in various metals exists. The percentage of excess ultrasonic attenuation in Na is 23.91%, in K 17.28 %, in Rb 29.28%, in Cs 26.68%, in Cd 28.55 %, in Sn 31.24 %, in Pb 24.17 %, in Bi 40.49%, in Hg 8.35%, in Zn 7.5% and in Ga 12.86%.

In Hg, however its value is only 9% of the classical value. This suggests that the ultrasonic attenuation in Hg is caused mainly by the classical processes of the ultrasonic attenuation, namely due to viscosity and thermal conductivity of the liquid mercury. Our value of excess ultrasonic attenuation in Hg, found using two-state model, gives twice of the experimental value. The reason for this discrepancy lies due to the uncertainty with the thermodynamic parameters used for the calculation of the ultrasonic attenuation due to classical processes.

Liquid zinc and gallium possesses vary small amount

Table 3–The values of excess ultrasonic attenuation (α/f^2) of the following liquid metals

Liquid Metal Metal	α / f^2 (10^{-17} Neper cm^{-1} s^2)			
	α / f^2 expt.	α_{Cl} / f^2 classical eq.(2)	α_B / f^2 excess = expt.– classical eq.(4)	α_B / f^2 present theory eq. (6)
Na	11.40	9.20	2.20	1.94
K	31.90	27.20	4.70	5.61
Zn	3.7±0.6	04.00	0.30	2.19
Ga	1.58±0.03	01.40	0.18	---
Rb	75.50	58.40	17.10	17.69
Cd	14.5±2.9	11.28	1.32	1.44
Sn	5.63±0.3	04.29	01.04	01.03
Cs	110.30	87.07	23.23	25.77
Hg	5.71±0.1	05.27	0.44	0.90
Pb	9.40±0.3	07.57	01.53	01.37
Bi	8.05±0.3	05.73	02.02	02.14

of excess ultrasonic attenuation. It appears that in these liquid metals the ultrasonic attenuation is caused mainly due to classical processes. However, our estimate of excess ultrasonic attenuation using two-state model gives a value, which is 7 times higher than that of the experimental value. In this case also, there is great amount of uncertainty in various thermodynamical parameters in liquid metals, hence perhaps this discrepancy.

Agreement of the results with experimental values indicates that this might be an appropriate approach to explain the excess attenuation of ultrasonic waves in liquid metals.

References

1 Awasthi O. N. and Murthy B. V. S., *Phys. Lett.*, 108A (1985) 119.
2 Murthy B. V. S. and Awasthi O. N., *Indian J. Pure & App. Phys*., 21 (1983) 540.
3 Hall L., *Phys. Rev.*, 73 (1948) 775.
4 Kor S. K., Rai G. and Awasthi O. N, *Phys. Rev.*, 186 (1969) 105.
5 Eyring H., *J. Chem. Phys*., 4 (1936) 283.
6 Ashcroft W. S. and Lekner J., *Phys. Rev.*, 145 83 (1966).
7 Stroud D. and Ashcroft N. W., Phys. Rev. B5 (1972) 371.
8 Sharma K. C., *Phys. Rev.*, 174 (1968) 309.
9 Vaid B. A. and Sharma K. C., *Phys. Stat. Sol*., (b) 125 (1984) 505.
10 Kim M. G., Kemp K. A. and Letcher S. V., *J. Acoust. Soc. Am.*, 49 (1971) 70.
11 Webber G. M. B. and Stephens R. W. S., *In*: *Physical Acoustics*, Vol. NB, ed. W.P. Mason (Academic Press, New York), p. 53 (1968).
12 Awasthi O. N. and Pundhir V. K., *Indian Journal of Pure and Applied Physics*, 45(5) (2007) 434–436
13 Kittel C., *Introduction to Solid State Physics* (7^{th} Edition), New York : John Wiley (2003).
14 Lide D. R., *CRC Handbook of Chemistry and Physics*, 80^{TH} Edition (New York) (1999-2000).
15 Bhatti S. S. and Singh D. P., *Ind. Jour. of Pure & Appl. Phys*., 20 (1982) 961.
16 Kaye G. W. C. and Laby T. H., *Tables of Physi. & Chemi. Const*. 15^{th} Edn., (New York) (1986).
17 Anderson O. L., *In*: *Physical Acoustics*, III B, ed. W. P. Mason, (Academic Press, New York) (1965) 84.
18 Smith P. A. and Smith C. S., *Phys. Chem. Solids*, 26 (1965) 279.
19 Koldarits F. J. and Trivisonno J., *Phys. Chem. Solids*, 29 (1968) 2133.
20 Roberts C. A. and Meister R., *Phys. Chem. Solids*, 27 (1966) 1401.
21 Murthy B. V. S. and Awasthi O. N., *Proc. II Western Pacific Regional Acoustic Conference*, Hong Kong (1985).
22 Sahu K. C., *Phys. Lett.*, 102A (1984) 370.
23 March N. H., *Liquid Metals* (Concepts and Theory), Cambridge University Press, (1990).

J. Pure Appl. Ultrason. 36 (2014) pp. 13-16

Ultrasonic emulsification: reduces droplet diameter and enhances stability

Vijayalakshmi Ghosh, Amitava Mukherjee and Natarajan Chandrasekaran

Centre for Nanobiotechnology, VIT University, Vellore-632014, Tamil Nadu, India
E-mail: nchandrasekaran@vit.ac.in

Nanoemulsions are colloidal dispersions of two immiscible liquids (oil and water) with droplet sizes between 20 and 200 nm. The efficient production of nanoemulsions with very low oil droplet sizes facilitates the inclusion of oil soluble bioactive substances into a range of water based foods and also in delivery of lipophilic drugs. Stability of nanoemulsion is one of the major concerns when we consider its applications. With exception to few (as in spontaneous emulsification), energy input is required to formulate nanoemulsion. In this present study, we assessed the effect of ultrasound on stability and droplet size of emulsion. The nanoemulsion formulated by emulsification time of 2 min, 5 min, 10 min and 15 min demonstrated stability for 1 day, 10 days, 30 days and 60 days respectively. Also we studied the performance of ultrasound emulsification with that of classical mechanical agitation. Coarse emulsion prepared by classical mechanical agitation, without being subjected for ultrasonic emulsification) exhibited phase separation within 2 hrs of preparation. Hence we conclude that emulsification time had a direct relation with the stability of nanoemulsion, which was due to the size reduction by ultrasound.

Key words: Basil oil, nanoemulsion, stability, ultrasonic emulsification, emulsification time.

Introduction

Nanoemulsions are submicron dispersions of oil and water with droplet size in the range of 10-100 nm[1]. Nanoemulsions have several potential advantages over conventional emulsions such as high physical stability, greater bioavailability and optical transparency which make them attractive systems for application in cosmetics, food and pharmaceutical industry. Nanoemulsions serve as delivery systems for oil soluble bioactive compounds such as drug, flavour, antimicrobial agents in the pharmaceutical and food industry respectively[2-5]. They have also found application in solubilizing sparingly water-soluble pesticides in agrochemical industry and for delivery of skincare and personal products in cosmetics[6-8].

Ultrasonic emulsification is one of the high energy methods to develop nanoemulsion. This method is reported as fast and efficient technique for preparing stable nanoemulsion formulations having very small droplet diameter with low value of polydispersity[9]. It utilizes high frequency sound waves (more than 20 kHz) to cause mechanical vibrations that lead to the formation of acoustic cavitation. These cavities gradually collapse and generate powerful shocks waves that break the micron range droplets of coarse emulsion to nanometric range[10]. Size of droplet diameter is optimized by taking into account the process parameters such as oil concentration, surfactant concentration, mixing ratio of oil and surfactant, viscosity of continuous phase, sonication time and energy input[11].

Formulation of nanoemulsion by ultrasonic emulsification has been reported by several works. But it was stable for few weeks only[12]. In our previous study, we studied the effect of process parameters on the droplet size of emulsion formulation[13]. Stability assessment of the formulated nanoemulsion plays a vital role before carrying out application studies. The objective of the present work is to analyze the stability of formulated nanoemulsion by studying the effect of emulsification time and droplet size.

Materials and methods

Materials

Basil oil (extracted from *Ocimum basilicum*) and Tween 80 were purchased from Sigma Aldrich, India. Deionised and Milli-Q (Millipore Corporation) water was used for all the experiments throughout the study.

Nanoemulsion preparation

Nanoemulsion was formulated using basil oil extracted

from *ocimum basilicum*, non-ionic surfactant Tween 80 (HLB-15) and water. Tween 80 was chosen to be used as emulsifier because it has a high hydrophilic and lipophilic balance value equal to 15 and favors the process of formulating oil-in-water type of emulsion. Tween 80 is non-ionic surfactant; hence it helps in stearic stabilization of emulsion droplets. Also, Tween 80 being a low molecular weight surfactant it is comparatively more efficient in minimizing droplet size than polymeric surfactants. Concentration of basil oil (6% v/v) was kept constant for all the nanoemulsion formulations. Coarse emulsion was prepared by mixing basil oil and surfactant (Tween 80) in different ratios (v/v) 1:1, 1:2, 1:3 and 1:4, and then water was added to the organic phase (Table 1). Coarse emulsion was then subjected to ultrasonic emulsification using Sonicator (20 kHz, 750W: Ultrasonics, USA). Energy input was given through sonotrode with a probe diameter of 13 mm. The probe generates intensive and disruptive forces to minimize droplet diameter of emulsion. Sonicator probe was symmetrically dipped into the beaker containing coarse emulsion, and the sonication process was done for different emulsification time. All the formulated nanoemulsions were characterized and stability of the emulsion was also investigated. Characterization of the formulated nanoemulsion was done in room temperature.

Characterization of nanoemulsion

Droplet size

Droplet size and polydispersity index (PDI) of the emulsion formulations were measured by 90 plus particle size analyzer. This instrument determines droplet size by dynamic light scattering technique. Nano-size droplets undergo Brownian motion in emulsion and hence, the intensity of scattered light will vary depending on droplet diameter. This intensity fluctuation in scattered light is measured by the dynamic light scattering technique. The droplet radius (R) can be calculated from Stokes-Einstein equation (Eq. (1)):

$$D = kT/6\eta R$$

where, D is the translational diffusion coefficient, k is the Boltzmann's constant, T is absolute temperature and η is the viscosity of the medium. Nanoemulsion formulations were diluted with milli-Q (Millipore corporation) water prior to experiment to avoid the effect of viscosity caused on account of emulsion ingredients and also to trim down the multiple scattering effect.

Stability of nanoemulsion

Centrifugation

The formulated nanoemulsions were studied for their resistance to centrifugation. All the formulations were subjected to centrifugation at 10,000 rpm for 30 min and observed for phase separation, creaming and cracking (if any).

Heating-cooling cycle

This study was done to check the effect of variation in temperature on the stability of nanoemulsion formulations. Samples were stored between temperature of 4 and 40°C each for a period of not less than 48 h. This cycle was repeated four times. The nanoemulsion formulations which did not show any instability (cracking, creaming and phase separation) were selected and subjected to freeze-thaw stress.

Freeze-thaw cycle

In this study, nanoemulsion formulations were subjected to freeze-thaw stress between –21 and +25 °C alternatively with storage at each temperature for 48 h as a minimum period. Three freeze-thaw cycles were performed.

Kinetic stability

Nanoemulsion formulations were stored at room temperature for studying intrinsic stability. The emulsion formulations were observed for phase separation, creaming and cracking with respect to prolonged storage

Table 1–Percent composition of different components of basil oil nanoemulsionsuspensions of stearic acid at 303 K

Formulation code	Oil : Surfactant (v/v)	Percent composition of different components			Droplet size (emulsification time = 15 min)
		Basil oil	Tween 80	Water	
BF1	1:1	6	6	88	41.15 nm
BF2	1:2	6	12	82	31.65 nm
BF3	1:3	6	18	76	29.60 nm
BF4	1:4	6	24	70	29.30 nm

time period. Kinetic stability was investigated by measuring droplet size of the nanoemulsions in different storage time.

Results and Discussion

Droplet size of nanoemulsion

Nanoemulsion formulated after emulsification period of 15 min showed droplet size of 41.15 nm, 31.65 nm, 29.6 nm and 29.3 nm for formulation code BF1, BF2, BF3 and BF4 respectively. Surfactant concentration demonstrated direct relation with droplet size.

Effect of emulsification time on droplet size of BF3 formulation was studied. With increase in emulsification time gradual decrease in droplet size was observed (Fig. 1). Emulsification time of 2 min, 5 min, 10 min and 15 min demonstrated droplet size of 99.5 nm, 45 nm, 32.3 nm and 29.6 nm respectively.

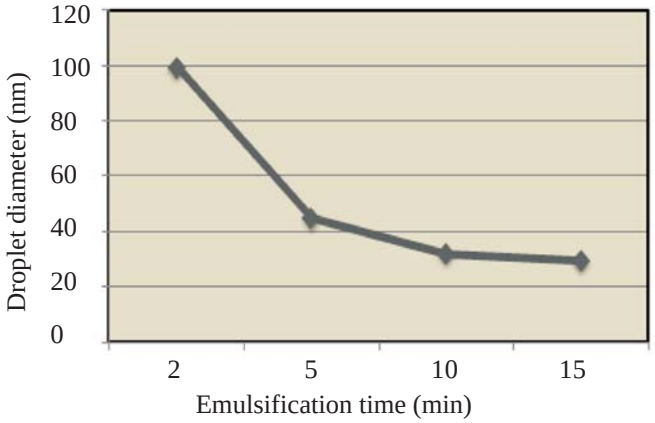

Fig. 1–Effect of emulsification time on droplet size of BF3 formulation

Stability of nanoemulsion

Centrifugation

All the formulated nanoemulsions after being sonicated were stable after being centrifuged for 30 min at 10,000 rpm (Table 2). All the coarse emulsions before subjecting to ultrasonic emulsification got phase separated after centrifugation.

Heating-cooling cycle

Nanoemulsion formulations such as BF2, BF3 and BF4 were stable to heating cooling cycle whereas their respective coarse emulsions before sonication got phase separated. BF1 formulation was not stable to heating-cooling cycle even after sonication (Table 2).

Freeze-thaw cycle

Nanoemulsion formulations such as BF3 and BF4 were stable to freeze-thaw stress whereas their respective coarse emulsions prepared by mechanical agitation (without subjecting to ultrasonic emulsification) demonstrated physical separation into constituent phases. BF1 and BF2 nanoemulsion formulations showed instability to freeze-thaw stress even after being sonicated (Table 2).

Kinetic stability

Physical separation was observed after 15 days of preparation in case of BF1 formulation and 30 days in case of BF2 formulation. No phase separation was observed in BF3 formulation even after 60 days (Table 3).

Nanoemulsion (BF3) was selected for kinetic stability study due to its low droplet size with low surfactant concentration. BF4 nanoemulsion formulated by emulsification time of 2 min, 5 min, 10 min and 15 min

Table 2–Thermodynamic stability of basil oil nanoemulsion (√ = stable samples and x = unstable samples)

Formulation code	Centrifugation (10000 rpm, 30 min)		H-C*		F-T**	
	Before sonication	After sonication	Before sonication	After sonication	Before sonication	After sonication
BF1	x	√	x	x	x	x
BF2	x	√	x	√	x	x
BF3	x	√	x	√	x	√
BF4	x	√	x	√	x	√

*Heating-Cooling cycle
**Freeze-thaw cycle

demonstrated stability for 1 day, 10 days, 30 days and 60 days respectively (Table 4).

Table 3–Kinetic stability of basil oil nanoemulsion (√ = stable samples and x = unstable samples)

Formulation code	Day 15	Day 30	Day 45	Day 60
BF1	x	x	x	x
BF2	√	x	x	x
BF3	√	√	√	√
BF4	√	√	√	√

Table 4–Effect of emulsification time on stability of BF3 nanoemulsion (√ = stable samples and x = unstable samples)

Emulsification time	Day 2	Day 10	Day 30	Day 60
2 min	x	x	x	x
5 min	√	x	x	x
10 min	√	√	x	x
15 min	√	√	√	√

Conclusion

Basil oil based nanoemulsion was formulated with droplet diameter of 29.6 nm (BF3 formulation) which was stable for 60 days. Emulsification time and droplet size showed direct relation with stability of the formulated nanoemulsion.

References

1 McClements D. J., Edible nanoemulsions: fabrication, properties, and functional performance, *Soft Matter,* **7** (2011) 2297-2316.

2 Kumar M., Misra A., Babbar A. K., Mishra A. K., Mishra P. and Pathak, Intranasal nanoemulsion based brain targeting drug delivery system of risperidone, *Int. J. Pharm.,* 358 (2008) 285-291.

3 Mou D., Chen H., Du D., Mao C., Wan J., Xu H. and Yang X., Hydrogel-thickened nanoemulsion system for topical delivery of lipophilic drugs, *Int. J. Pharm.*, 353 (2008) 270-276.

4 Li P. and Chiang B., Process optimization and stability of D-limonene-in-water nanoemulsions prepared by ultrasonic emulsification using response surface methodology, *Ultrason. Sonochem.*, 19 (2012) 192-197.

5 McClements D. J., Decker E. A. and Weiss J. J., Emulsion-based delivery systems for lipophilic bioactive components, *J. Food Sci.,* 72 (8) (2007) R109-R124.

6 Wang L., Li X., Zhang G., Dong J. and Eastoe J., Oil-in-water nanoemulsions for pesticide formulations, *J. Colloid Interface Sci.*, 314 (2007) 230-235.

7 Sonneville-Aubrun O., Simonnet J. T. and L'Alloret F., Nanoemulsions: a newvehicle for skincare products, *Adv. Colloid Interface Sci.*, 108-109 (2004) 145-149.

8 Konga M., Chenb X. G., Kweonc D. K. and Park H. J., Investigations on skin permeation of hyaluronic acid based nanoemulsion as transdermal carrier, *Carbohydr. Polym.*, 86 (2011) 837-843.

9 Lin C. and Chen L., Comparison of fuel properties and emission characteristics of two- and three-phase emulsions prepared by ultrasonically vibrating and mechanically homogenizing emulsification methods, *Fuel*, 87 (2008) 2154-2161.

10 Behrend O., Ax K. and Schubert H., Influence of continuous phase viscosity on emulsification by ultrasound, *Ultrason. Sonochem.*, 7 (2000) 77-85.

11 Nakabayashi K., Amemiya F., Fuchigami T., Machida K., Takeda S., Tamamitsub K. and Atobe M., Highly clear and transparent nanoemulsion preparation under surfactant-free conditions using tandem acoustic emulsification, *Chem. Commun*., 47 (2011) 5765-5767.

12 Li P. and Chiang B., Process optimization and stability of D-limonene-in-water nanoemulsions prepared by ultrasonic emulsification using response surface methodology, *Ultrason. Sonochem.*, 19 (2012) 192-197.

13 Ghosh V., Mukherjee A. and Chandrasekaran N., Ultrasonic emulsi?cation of food-grade nanoemulsion formulation and evaluation of its bactericidal activity, *Ultrason. Sonochem.,* 20 (2013) 338-344.

J. Pure Appl. Ultrason. 36 (2014) pp. 17-24

Studies on solid lipid nanoparticles (SLN) of stearic acid-effect of particle size and degree of dispersion on ultrasonic velocity

G. Cynthia Jemima Swarnavalli[1], D. Roopsingh[2], V. Joseph[3] and V. Kannappan[2]

[1]Department of Chemistry, Women's Christian College, Chennai, Tamil Nadu
[2]Department of Chemistry, Presidency College, Chennai
[3]Department of Physics, Loyola College, Chennai
E-mail: cynprin@gmail.com

In view of the importance of solid lipid nanoparticles (SLN) as novel delivery systems for pharmaceutical and cosmetic active ingredients, ultrasonic velocimetry was used to study nano suspensions of SLN. The propagation of sound through colloidal systems can probe new properties that characterize both structure and the dynamics of the suspension. Stearic acid (SA) a biocompatible fatty acid was made into SLN by nano precipitation method. In order to have solid lipid nanoparticles of varied sizes, two stabilizer systems, a mixture of cetyl trimethylammonium bromide (CTAB) and 0.3% solution of poly (vinylpyrrolidone) (PVP) (Mw 40 k Da) (stabilizer-I) and a mixture of polyoxyethylene sorbitan fatty acid ester (TWEEN-80) and anionic surfactant sodium dodecyl sulphate (SDS) (stabilizer-II) were used. A correlation between crystallinity of the SLN, particle size and ultrasonic velocity was realized. Dispersion stability was found to be related to certain acoustic parameters. A comparison of effective density and velocity computed according to three theoretical models viz. Urick, Kuster and Toksöz and Urick and Ament was made with experimental values.

Keywords: SLN, stearic acid, stabilizing agents, crystallinity, DLS, DSC, TEM, SEM, ultrasonic velocity, compressibility

Introduction

Solid lipid nanoparticles (SLN) were developed by Muller in the 1990's. They find application in drug and cosmetic delivery along with liposomes, micro emulsions and polymeric nanoparticles. However, a clear advantage of SLN over the above mentioned colloidal delivery systems are the fact that the lipid matrix is made from physiological lipids, which decrease the danger of acute and chronic toxicity[1-4]. Due to their numerous advantages over existing conventional formulations, SLN have been introduced as a novel carrier system for the controlled release of pharmaceutical and cosmetic active compounds[5,6]. SLN enhances *in-vivo* skin hydration through occlusive property. Occlusive effect of solid lipid nanoparticle is controlled by particle size, sample volume, lipid concentration and crystallinity of the lipid matrix[7, 8]. Solid lipid nanoparticles have potentially lucrative application in topical cosmetic products[9].

Wissing and Muller[10] have shown that SLN are physically stable in aqueous suspensions and also after incorporation into a dermal cream thus combining the advantage of existing cream with that of the SLN. The occlusion promotes the penetration of actives such as vitamin E[11] and retinyl palmitate[12] into the skin. SLN were also established as an UV protection system[13]. The particles themselves may act as UV blocker due to their particulate character.

Ultrasonic velocity measurements in lipid suspensions are rarely reported. Ultrasonic action is one of the most promising methods of influence on the behaviour of ensembles of colloidal and nanoparticle solutions. Such measurements offer a means of determining volume fractions or compressibilities of dispersed phases in many systems and in special cases may even be used as a means of particle sizing and determining dispersed or continuous phase viscosities. In the present work, an attempt was made to use ultrasonic velocimetry to determine the compressibility of SLN of stearic acid and their degree of dispersion in aqueous suspension. The degree of dispersion influences suspension stability and hence sound velocity. Increase in the degree of dispersion in a suspension involves a decrease in the absorption coefficient, which allows the estimation of efficiency of the stabilizer[14]. A comparison of effective density and

velocity computed according to three theoretical models *viz*. Urick, Kuster and Toksöz and Urick and Ament with experimental values were also made. The solid lipid nano particles are characterized by measuring their particle size, size distribution kinetics (zeta potential), degree of crystallinity and surface morphology. In addition to these, the compressibility of the SLN in aqueous medium and effect of particle size on ultrasonic velocity are discussed in the present work.

Theoretical Considerations

The Urick equation

The Urick equation[15] is probably the simplest and most widely used equation for predicting velocity of sound in suspensions and emulsions. The overall equation for predicting the velocity can be written as follows:

$$U = [((1-\varphi)\rho_1+\varphi\rho_2)\ ((1-\varphi)\kappa_1+ \varphi\kappa_2)]^{-1/2} \quad (1)$$

where,

U = Velocity of sound through the suspension

ρ = Density of the suspension

κ = Compressibility of the material (subscripts 1 and 2 indicate the continuous and dispersed phases respectively)

In the case of dilute suspensions, volume averaged values of ρ and κ are inserted in Eq. (1), (i.e.)

$$\kappa_{eff} = (1-\varphi)\rho_1 + \varphi\kappa_2 \quad (2)$$

$$\rho_{eff} = (1-\varphi)\ \rho_1 + \varphi\kappa_2 \quad (3)$$

where,

φ = Particle volume fraction and the subscripts 1 and 2 indicate the continuous and dispersed phases respectively. The particle volume fraction of the particles were calculated using the equation,

$$\varphi = \rho_o - \rho_1/ \rho_2 - \rho_1 \quad (4)$$

where, ρ_o, ρ_1 and ρ_2 are density of the suspension, continuous medium and suspended particle respectively.

The Kuster and Toksöz equation

Kuster and Toksöz[16] used a scattering approach. Their simplified expression for a dilute suspension was given by

$$\rho_{eff} = \rho_1[(2 + \varphi)\ \rho_2 + (1 - \varphi)\ \rho_1]/[2(1 - \varphi)\ \rho_2+ (1 + 2\varphi)\ \rho_1] \quad (5)$$

$$U = (\kappa\ \rho_{eff})^{-1/2}$$

Both Urick and Kuster and Toksöz equation need the same parameters to predict velocity of sound.

The Urick and Ament equation

Urick and Ament[17] gave a more general equation using scattering approach (similar to Kuster) where they assumed the composite media consists of small randomly located particles embedded in a continuous fluid. The simplified form of Urick and Ament equation is

$$U = \{[\kappa(\rho_1(1+\varphi\sigma)[X\ (\sigma+X) + Y^2)]/[(\sigma+X)^2 +Y^2]\}^{-1/2} \quad (6)$$

where $\sigma = \rho_2 - \rho_1/\rho_1$

$X = 3(1+1.5Ba)/2$

$Y = [9(1+ 1/Ba)]/4Ba$

where B=1/d and d= $(2\eta/ 2\pi\nu\rho)^{1/2}$ and ν is the frequency of sound used which is 2MHz , ρ and η are the density and viscosity of the continuous medium respectively. 'a' is the particle diameter.

Acoustic parameters

The formulae used for the calculation of acoustic parameters such as adiabatic compressibility (κ), acoustic impedance (Z) and absorption coefficient (α/f^2) are given below. The experimentally determined parameters velocity, density and viscosity are made use of in calculation of these parameters.

$$\kappa = [1/ U^2\rho] \quad (7)$$

$$Z = U\ \rho \quad (8)$$

$$\alpha /f^2 = (8\times3.14\times3.14\times\eta)\ /3\rho U^3 \quad (9)$$

Experimental Methods

Materials

Merck samples of Stearic acid, CTAB, PVP and SDS and TWEEN-80 (Aldrich chemicals) were used as such without further purification.BDH samples of acetone, tetrahydrofuran (THF), acetonitrile, and ethanol were used after purification.

Preparation of suspensions of SLN of stearic acid

Solid lipid nanoparticles were prepared by nanoprecipitation technique proposed by Fessi *et al*[18]. The two stabilizer systems used were a mixture of cetyl trimethylammonium bromide (CTAB) and 0.3% solution of poly (vinylpyrrolidone) (PVP) (Mw 40 k Da) (stabilizer-I) and a mixture of polyoxyethylene sorbitan fatty acid ester (TWEEN-80) and anionic surfactant sodium dodecyl sulphate (SDS) (stabilizer-II). The method is defined as follows: On the one hand 125 mg of stearic acid was dissolved in a mixture of solvents (total volume 20 mL) (Table 1). On the other hand specified amount of the stabilizer was dissolved (25 ml) in double distilled water. The organic phase was added to the aqueous phase with magnetic stirring (200 rpm) at room temperature. The mixture immediately became

Table 1–Preparation parameters and physico chemical characteristics of the stearic acid (SA) nanoparticles

Parameters	SA-1	SA-2	SA-3	SA-4	SA-5	SA-6
Water (mL)	25	25	25	25	25	25
Acetone (mL)	18			18		
Ethanol (mL)		20			20	
Acetonitrile (mL)			15			15
Tetrahydrofuran (THF)	2		5	2		5
CTAB (mL)	2	2	2			
PVP (mL)	2	2	2			
TWEEN-80 (mL)				0.5	0.5	0.5
SDS (mL)				0.3	0.3	0.3
Mean particle size obtained from DLS z_{ave} (nm)	271.6	205.1	355.8	320.0	323.5	323.5
Particle size obtained from SEM/TEM (nm)	180-220	150-160	110	250	216.6	300
M.pt from DSC measurement(°C)	61.1	64.2	60.9	54.1	59.5	52.4
Enthalpy of formation (J/g)	181.3	86.17	140.9	49.75	70.82	35.75

opalescent as a result of the formation of lipid nanoparticles. The nanosuspension was formed instantaneously and stirred during an additional time of 5-10 minutes. The organic solvents were removed under reduced pressure leaving the aqueous suspension. The preparation parameters (solvent compositions and stabilizers) of the six batches of stearic acid nanoparticles, their characterization and physicochemical studies, are presented in Table 1.

Measurement of ultrasonic velocity

The aqueous suspension containing solid lipid nanoparticles was diluted into various dilutions (0.13 to 1.0 volume fraction) by sonication for 3 minutes in an ultrasonic bath (Pci ultrasonic bath sonicator 1.5 L). The densities of the continuous medium (water-stabilizer) and suspensions have been determined in a specific gravity bottle of 10 mL capacity using a single pan electrical balance with an uncertainty of ±0.1 mg. The particle volume fractions were calculated using Eq. (4). Viscosity of the mixtures was measured using an Ostwald's viscometer with an accuracy of ± 0.001. The speed of sound was measured by a single frequency ultrasonic interferometer operating at 2 MHz with an accuracy of ± 0.1 m/s. Precautions were taken to exclude air bubbles in the suspension throughout all the measurements. The temperature of the solution was maintained at 303±0.1K by circulating water through the jacket of the double walled cell from a thermostatic water bath.

Characterization of SLN

The morphology and size of the SLN (SA-1 to SA-6) were examined using a high resolution scanning electron microscope and an electronic transmission microscope at 80 kV. The observation was made after 50-fold dilution with the original dispersion medium of the preparation; the samples were negatively stained with 1% (w/v) phosphotungstic acid.

The mean particle size was analyzed using dynamic light scattering (DLS), also known as photon correlation spectroscopy (PCS). PCS is a light-scattering technique that is used to obtain the hydrodynamic diameter (z-average) and the polydispersity index (PI), which is a measure of the width of the particle size distribution. Prior to the measurement, all samples were diluted using ultra-purified water to yield a suitable scattering intensity. Samples were analyzed at 25°C using the general purpose mode.

The stability of the SLN suspensions was assessed by zeta potential measurements by applying a field strength of 20 V/cm. The zeta sizer measures the electrophoretic mobility of the particles, which was converted into the zeta potential using the Helmholtz-Smoluchowski equation built into the software.

The X-ray diffraction patterns were determined for the lyophilized samples stearic acid SLNs (SA-1 to SA-6). Powder X-ray diffraction (XRD) patterns were measured using powder diffractometer, using nickel filtered copper K-alpha radiations (λ=1.5461Å) with a scanning rate of 0.02°. The diffraction pattern was recorded in the range of 5-70°.

The FT IR spectra of lyophilized stearic acid SLN (SA-1-SA-6) samples were recorded by Perkin Elmer spectrum one FTIR spectrometer. Thermograms were recorded with a differential scanning calorimeter Samples

were heated at the scanning rate of 3°C/min over a temperature range between 30 and 100°C.

Results and Discussion

Size, morphology and crystallinity of the SLN

According to HRSEM/TEM pictures, the particles have a smooth surface and are spherical, and the majority of the particles do not exhibit aggregation between them. All the six formulations of SA SLN have varied size and were crystalline as seen from the XRD pattern which is in agreement with the literature values of the crystal structure of stearic acid. The SLN formulation prepared with stabilizer system-I are more crystalline in comparison with the SLN formulations prepared with stabilizer system-II as seen from the XRD. The average particle size of the different batches of stearic acid SLN (SA-1 to SA-6), as determined by dynamic light scattering (DLS) and SEM/TEM are given in Table-1. The particle size of the SLN suspension produced with cationic surfactants (stabilizer -I) is considerably smaller compared to nonionic formulations. Such behaviour has been reported in literature by Wolfgang *et al*.[19]. The zeta potential values from -8.3 mV and+29 mV indicate moderate stability of the SA SLN with limited flocculation[20]. The physical state of the dispersed particles of the SLN is understood via the characteristic melting or transformation endotherms upon heating. Stearic acid nanoparticles in suspension SA-1 to SA-6 show a well defined endothermic peak at a temperature lower than the melting point of the bulk stearic acid crystals. This indicates that stearic acid nanoparticles are in the crystalline state. Presence of a single peak indicates the absence of other lipid modifications. The DSC measurements indicate that the melting point of the stearic acid particles prepared with TWEEN-80 and SDS (52.4-59.5 °C) are lower than that of the nanoparticles prepared with PVP and CTAB (60.9 -64.2 °C). Thus it is clear that the stabilizer -II (TWEEN-80 and SDS) reduces the crystallinity and melting point of the SA SLN formulations. The FTIR spectra of the six samples were recorded. All the characteristic absorption bands are broadened at certain characteristic frequencies indicating the formation of nanoparticles. The DLS average particle size (z_{av}), Poly dispersity index (P.I), distribution intensity and zeta potential of the six formulations of stearic acid SLN are given in Table 2. It is seen from the SEM/TEM images that all the six suspensions consist mostly of spherical particles and are moderately monodispersed.

Comparison of theory and experiment

The density and velocity measured in the SLN suspension has been compared with the theoretical values calculated from Urick, Urick and Ament, and Kuster and Toksóz equations. Comparison of theoretical and experimental densities as a function of volume fraction is given in Fig. 1 (A-F). The predictions of effective density according to Urick and kuster and Toksöz model agree exactly with experimentally determined densities for the SLN suspensions. Such good agreement between effective densities calculated and experimental values is reported in the case of silver sol[21]. It is of interest to note that these two equations agree exactly with each other. But this is in contrast with the silver sol and suspensions where the Urick and Urick and Ament equations agreed well and Kuster and Toksöz was a poor model. It is also seen that the Urick and Ament model in this case predicts poorly.

The velocity graphs show a different picture. The velocity predictions of the three models do not agree with the experimental velocities at very low and higher volume fractions. However there is a close agreement with Urick and Kuster and Toksöz equations at certain intermediate volume fractions of the suspensions. This is also in contrast with the behaviour of metal nanoparticles where

Table 2–Particle size, polydispersity index and zeta potential of stearic acid SLN

SLN	Size (nm)	Distribution intensity	Poly dispersity index	Cummulative fit error	Zeta potential (mV)
SA-1	271.6	100	0.772	0.00772	-18.3
SA-2	205.1	100	0.773	0.0188	-12.6
SA-3	355.8	100	0.399	0.00293	+29.0
SA-4	322.9	96.7	0.595	0.0033	-13.5
SA-5	320.0	100	0.404	0.00105	-16.0
SA-6	323.5	93.1	0.350	0.00173	-8.3

the more general Urick equation predicted well[21]. Comparison of theoretical and experimental velocities as a function of volume fraction is given in Fig. 2 (A-F). Ultrasonic velocity calculated according to the Urick and Kuster and Toksöz equations give very similar predictions across the whole range of volume fraction of the suspensions. In the suspensions made with stabilizer - II, the experimental velocities are lower than the theoretical predictions which may be due to increase in viscosity of the suspensions with volume fraction. Such lower values are normally attributed to scattering of sound by particles[22].

However, in this case it may not be due to scattering of sound since the particles are very small and in this case less crystalline. In the case of the suspension SA-6 (average size 300 nm), the experimental velocities lie much lower than theoretical predictions. This may be due to larger particles in this particular suspension. The density difference between the suspended particle (Stearic acid (ρ) = 847.0 kg/m^3,) and the continuous medium (water ρ = 995.65 kg/m^3) is not appreciable. However the (Ba) terms are larger compared to that of the metal nanoparticles, and hence it decreases the velocity. However the homogeneity condition which was well satisfied by the metal nanoparticle (8 nm to 35 nm) suspensions 21 seem not to be applicable in the case of suspension with particle size >100 nm. This may be due to the vast difference in the compressibility between the metal nanoparticles and lipid nanoparticles.

Acoustic parameters

The measured ultrasonic velocity and computed adiabatic compressibility, acoustic impedance and absorption coefficient are given in Tables.3 &4 respectively. It is of interest to note that the experimental ultrasonic velocity increases up to a particular volume fraction and then decreases. The same trend is shown by all the six suspensions (Table 3). The order of ultrasonic velocity among the suspensions is as follows: SA-2 > SA-1 > SA-3 > SA-5 > SA-4> SA-6. It was observed that as far as ultrasonic velocity is concerned more crystalline the SLN more is the velocity of sound. It was also observed that the suspensions with smaller particles have greater velocity than suspensions with larger particles. The decrease in ultrasound velocity at higher suspension concentration can be explained by hydrodynamic dispersion since scattering can be neglected for these very small particles. On comparing the compressibility of SLN in the six suspensions it is in

Table 3–Experimental velocity (U) and computed acoustic parameter adiabatic compressibility(κ) of the six SLN suspensions of stearic acid at 303K

Vol.	Ultrasonic velocity						(U) m/sAdiabatic compressibility (κ) N^{-1} m^2					
fraction	SA-1	SA-2	SA-3	SA-4	SA-5	SA-6	SA-1	SA-2	SA-3	SA-4	SA-5	SA-6
0.133	1516.2	1518.5	1514.6	1500.0	1510.0	1504.2	4.37	4.36	4.39	4.45	4.39	4.43
0.266	1520.3	1522.4	1519.2	1502.8	1512.2	1500.8	4.34	4.33	4.34	4.43	4.39	4.45
0.400	1524.7	1524.7	1522.4	1510.2	1516.8	1505.4	4.32	4.32	4.36	4.39	4.37	4.44
0.533	1515.2	1527.6	1516.9	1512.4	1518.8	1502.3	4.37	4.30	4.38	4.39	4.36	4.46
0.666	1513.6	1513.6	1514.1	1505.8	1514.0	1501.2	4.38	4.39	4.39	4.44	4.38	4.46
0.800	1511.2	1512.2	1511.6	1504.3	1511.4	1501.0	4.39	4.40	4.40	4.45	4.39	4.46
1.000	1500.8	1505.8	1506.4	1501.4	1509.0	1499.4	4.46	4.44	4.42	4.46	4.40	4.47

Table 4–Computed acoustic parameters acoustic impedance, absorption coefficient and adiabatic compressibility of the six SLN of stearic acid at 303K

Vol.	Acoustic Impedance 10^3 kg m^2 s^{-1}						Absorption Coefficient 10^{-15} (α/f^2)Npm^{-1} s^2					
fraction	SA-1	SA-2	SA-3	SA-4	SA-5	SA-6	SA-1	SA-2	SA-3	SA-4	SA-5	SA-6
0.133	150.95	151.13	150.47	149.73	150.79	150.15	5.64	5.69	5.75	5.81	5.69	5.80
0.266	151.40	151.58	151.52	150.21	150.74	149.59	5.78	5.71	5.75	6.01	5.66	5.91
0.400	151.88	151.86	150.77	150.98	150.84	149.67	5.77	5.73	5.80	5.73	5.65	5.90
0.533	150.98	152.12	150.61	150.64	150.94	149.35	5.89	5.72	6.48	6.06	5.64	6.25
0.666	150.72	150.58	150.48	149.61	150.80	149.20	5.94	5.98	6.26	6.09	5.73	6.46
0.800	150.67	150.43	150.46	149.31	150.60	149.39	6.07	6.11	6.61	6.13	5.86	6.02
1.000	149.51	149.67	150.15	149.39	150.53	149.10	6.25	6.24	6.77	6.05	6.02	5.99

the order SA-6 > SA - 4 > SA- 5 > SA - 3 > SA -1 > SA-2. There is a minimum in the compressibility curve very much similar to that of the silver sol and suspension[21]. The compressibility order is the opposite of crystallinity order of the SLN. Compressibility shows a nonlinear variation with volume fraction. However at higher volume fractions, compressibility of all the six samples tends to increase. In aqueous medium there is significant solvation and that may be the reason for increasing compressibility of the SLN. This study also shows that at higher concentration acoustic impedance tend to decrease, which indicates that as volume fraction increases hindrance to sound propagation also increases.

Increase in the degree of dispersion in a suspension involves a decrease in the absorption coefficient, which allows the estimation of efficiency of the dispersive agent. When we analyze the variation of absorption coefficient of the six SLN suspensions with volume fraction (Table 4), we observe that it increases with particle volume fraction indicating the degree of dispersion decreases with volume fraction. It is also noted that the absorption coefficient of SLN suspensions SA-2 and SA-5 is the lowest among the six formulations with a minimum which is an indication of increase in degree of dispersion, this is also confirmed by the zeta potential values (SA-2ζ-12.6mV and SA-5 ζ -16 mV). Absorption coefficient for SA-1 and SA-4 shows minima at the same particle volume fractions. The SLN SA-3 (ζ 29 mV) and SA-6 (ζ -8.3 mV) in spite of showing minima at lower volume fraction shows a peak at higher volume fractions, and thus indicates the degree of dispersion is low at higher volume fractions. The increase in absorption coefficient with volume fraction may be attributed to the incomparable vibrational amplitude of the suspended SLN and the dispersion medium. An interesting correlation was noticed among the SA SLN, that SLN with same composition of solvents behave similarly i.e the trend in variation of absorption coefficient with volume fraction is similar.

Conclusion

Six formulations of Stearic acid nanoparticle suspensions were prepared with mixture of solvents and a combination of stabilizers. The SLN prepared with CTAB and PVP(stabilizer-I) was found to be smaller in size, more crystalline and has higher melting point in comparison with the SLN prepared with TWEEN-80 and SDS as emulsifier. Ultrasonic velocity measurements in these suspensions reveal that all the suspensions show

an increase in velocity up to an intermediate volume fraction and then decreases as volume fraction increases. The trend is similar in all the suspensions. An interesting correlation between crystallinity and ultrasonic velocity was realized. Higher the crystallinity of the SLN is, the higher is the ultrasonic velocity in the suspension. This is further confirmed by the values of compressibility of the suspended lipid particle in the suspensions which is inversely related to velocity. Compressibility increases with decreasing crystallinity (SA-2 < SA-1 < SA-3 < SA-5 <SA-4 < SA-6). From the thermo grams of the six SLN it was found that the SLN prepared with TWEEN-80 and SDS(stabilizer-II) is having lower melting points compared to the SLN prepared with CTAB and PVP (stabilizer-I). The ultrasonic velocity in these suspensions (SA-4, 5 & 6) is lower than the other three suspensions. This may probably due to the larger size and decreasing crystalline nature of the SLN. Absorption coefficient curves show minima for suspensions with smaller and more crystalline SLN. Another interesting observation is that the trend in variation of absorption coefficient with volume fraction is similar for suspensions having the same set of solvents. A comparison of experimental density and velocity was made with three theoretical equations *viz*, Urick, Urick and Ament, and Kuster and Toksóz. It was observed that the suspensions come under the viscous regime. Ultrasonic velocimetry is also used to compute the compressibility of the suspended lipid nanoparticle in the suspension. In this study, Ultrasonic velocity measurements show how the velocity depends on particle size and crystallinity. Highly dispersed suspensions containing crystalline SLN show lower absorption coefficient and higher ultrasonic velocity. In view of the importance of SLN in drug delivery and cosmetics, this fact may be helpful in assessing the performance of the solid lipid nanoparticles.

Acknowledgement

One of the authors (GC) is grateful to University Grants Commission (UGC), New Delhi, India for the award of Teacher Fellowship under the Faculty Development Programme (FDP). The authors thank Dr.John Philip, Head, Smart section, NDE, IGCAR, Kalpakkam, Chennai, India for measurement of zeta potential of the nanosuspensions.

References

1 Hou D., Xie C., Huang K. and Zhu C., The production and characteristics of solid lipid nanoparticles (SLNs), *Biomaterials*, 24 (2003) 1781-1785.

2 Souto E. B., Wissing S. A., Barbosa C. M. and Müller R. H., Development of a controlled release formulation based on SLN and NLC for topical clotrimazole delivery. *Int. J. Pharm.*, 278(2004) 71- 77.

3 Chan J. M., Valencia P. M., Zhang L., Langer R. and Farokhzad O. C., Polymeric nanoparticles for drug delivery, Methods. *Mol.Biol.*, 624 (2010) 163-175

4 Mehnert W. and Mader K., Solid lipid nanoparticles Production, characterization and applications, *Adv. Drug. Del. Rev.*, 47 (2001) 165-196.

5 Muller R. H., Schwarz C., Mehnert W. and Lucks J. S., Production of solid lipid nanoparticles (SLN) for controlled drug delivery, *Proc. Int. Symp. Control. Rel. Bioact Mater.*, 20 (1993) 480-481.

6 R. H. Muller and A. Dingler, The next generation after the liposomes: solid lipid nanoparticles (SLN/ Lipopearls) as dermal carrier in cosmetics, *European Cosmetics*, 7 (1997) 19-26.

7 Wissing S. A. and Mu¨ller R. H., The influence of the crystallinity of lipid nanoparticles on their occlusive properties, *Int. J. Pharm.*, 242 (2002) 377-379.

8 S. A. Wissing and R. H. Muller Cosmetic applications for solid lipid nanoparticles(SLN), *Int. J. Pharm.*, 254 (2003) 65-68.

9 LippacherA., Muller R. H. and Mader K., Semisolid SLN(TM) dispersions for topical application: influence of formulation and production parameters on viscoelastic properties, *Eur. J. Pharm. Biopharm.*, 53 (2002)155-160.

10 Wissing S. A. and Muller R. H., The influence of solid lipid nano particles on skin hydration and viscoelasticity - *in vivo* study, *Eur. J. Pharm. Biopharm.*, 56 (2003) 67-72.

11 Dingler A., Blum R. P., Niehus H., Müller R. H. and Gohla S. H., Solid lipid nanoparticles (SLN/ lipopearls)- A pharmaceutical and cosmetic carrier for the application of vitamin E in dermal products, *J. Microencapsulation.*, 16 (1999)751-767.

12 Saupe A. and Thomas R., Nanocarrier Technologies In Frontiers of Nanotherapy; Reza Mozafari., Ed.; (Springer, The Netherlands, 2006).

13 Jenning V., Gysler A., Schafer-Korting M. and Gohla S. H., Vitamin A loaded solid lipid nanoparticles for topical use: occlusive properties and drug targeting to the upper skin, *Eur. J. Pharm. Biopharm.* 49 (2000) 211-218.

14 Piotrowska A., Propagation of ultrasonic waves in suspensions and emulsions 2. Relation between

ultrasonic properties and certain characteristics of the medium, *Ultrasonics.*, 9 (1971) 235-239.

15 Urick R. J., A sound velocity method for determining the compressibility of finely divided substances, *J. Appl. Phys*., 18 (1947) 983-987.

16 Kuster G. T. and Toksöz M. N.,Velocity and attenuation of seismic waves in two phase media, part-II Experimental results, *Geophysics,* 39 (1974) 607-618

17 Urick R. J. and Ament W. S., The propagation of sound in composite media, *J. Acoust. Soc. Am.*, 21 (1949) 115-119.

18 Curt F., Devissaguet Jean-Philippe, Puisieux Francis and Thies Curt, Process for the preparation of dispersible colloidal systems of a substance in the form of nanoparticles. US Patent, (1992) 5,118,528,

19 Mehnert W. and Mader K., Solid lipid nanoparticles Production, characterization and applications, *Adv. Drug Deliv. Rev.*, 47 (2001)165-196.

20 Heurtault B., Saulnier P., Pech B., Jacques-Emile Proust and Jean-Pierre Benoit, Physico-chemical stability of colloidal lipid particles, *Biomaterials* 24 (2003) 4283-4300

21 Cynthia Jemima Swarnavalli G., Joseph V., Roopsingh D. and Kannappan V., Studies on nano suspensions of silver sol and redispersed nanocrystallite silver in aqueous and alcoholic media, *J. Mol. Liq*., 164 (2011) 243-249.

22 Harri K. and Kytomaa, Theory of sound propagation in suspensions: a guide to size and concentration characterization, *Powder Technol*., 82 (1995) 115-121.

23 Horvath-Szabo G. and Høiland H., Compressibility Determination of Silica Particles by Ultrasound Velocity and Density Measurements on Their Suspensions, *J. Colloid Interface. Sci.*, 177 (1996) 568-578.

J. Pure Appl. Ultrason. 36 (2014) pp. 25-27

Binary mixtures of aniline with alkanols -an ultrasonic study

K. Sathi Reddy[1], D. Shanmukhi Jyothi[2] and D. Linga Reddy[3]

[1]Department of Physics, College of Natural Science, Arba Minch University, Ethopia.
[2]Department of Physics, Sardar Patel College, Secunderabad-500 025 (A.P), India.
[3]Department of Physics, UCS, Osmania University, Hyderabad-500 007, (A.P), India
E-mail : jyothi6physics@gmail.com

Ultrasonic velocity (v), density (ρ), refractive index(n) for binar y mixtures of aniline with ethanol, methanol, propanol have been measured at room temperature of about 300.15 K over entire volume component percentage range. The Ultrasonic velocity (v) is measured using Ultrasonic Pulse Echo Overlap (PEO) technique at a frequency of 2MHz. The density measurements have been carried out by using 10ml specific gravity bottle. Refractive index (n) measurements have been carried out by using Abbe Refractometer. Adiabatic Compressibility (β) and dielectric constant (s) were computed using measured data of density, ultrasonic velocity and refractive index.

Keywords: Ultrasonic velocity (v), aniline, adiabatic compressibility (β), ultrasonic pulse echo overlap technique

Introduction

Complex formation through hydrogen bonding plays an important role in characterizing the thermodynamic behavior of many associating type liquid binary systems. From the ultrasonic point of view the parameters of interest are ultrasonic velocity, density, adiabatic compressibility, refractive index and macro dielectric constant. Ultrasonic study[1-4] is a useful technique for understanding the phsico-chemical properties of the pure liquids and liquid mixtures. Ultrasonic measurements are extensively used to study the molecular interactions in pure liquids and liquid mixtures. Ultrasonic velocity has been subject of active interest during the recent years[5-7]. Nomoto and co-researchers made successful attempts to evaluate the sound velocity in binary mixtures.

The present study envisages the determination of ultrasonic velocity (v) density (ρ) and to compute the parameters like adiabatic compressibility (β), macro dielectric constant (ε) of a few alcohols like Methanol, Ethanol and Propanol in Aniline.

Experimental

Ultrasonic technique has been widely used for different types of investigation[8]. In Pulse Echo Overlap method, a short sinusoidal electrical wave activates the Ultrasonic transducer. The transducer then produces sound wave trains into the liquid inside the cell.

This cell is made up of stainless steel which avoids any chemical reactions between the chemicals and the cell. The Ultrasonic velocity was measured with the help of microprocessor based Ultrasonic Pulse Echo Overlap (PEO) technique at 2MHz frequency. The internal circuit of PEO is designed with solid state version and it has special memory features of permanent storage and direct digital read out of Ultrasonic velocity up to an accuracy of ±1m/s.

The densities of all the mixtures have been determined with 10ml. specific gravity bottle and mass (m) of a given volume of the liquid is determined by using a single pan opto-electrical balance. The results of the densities are accurate to ±0.5%.

The refractive index (n) of the mixture has been determined using an Abbe Refractometer with an accuracy of ±0.2%.

Results and Discussion

Ultrasonic velocity in different mixtures increases with increase in chain length of alcohols (Fig. 1) till 40% of alcohol concentration and beyond 40% of volume component there is a reversal trend indicating that the velocities are in the increasing trend of Ethanol > Propanol > Methanol. The reason may be thought as beyond 40% volume component of alcohol the higher homologue Propanol is functioning in coiled manner

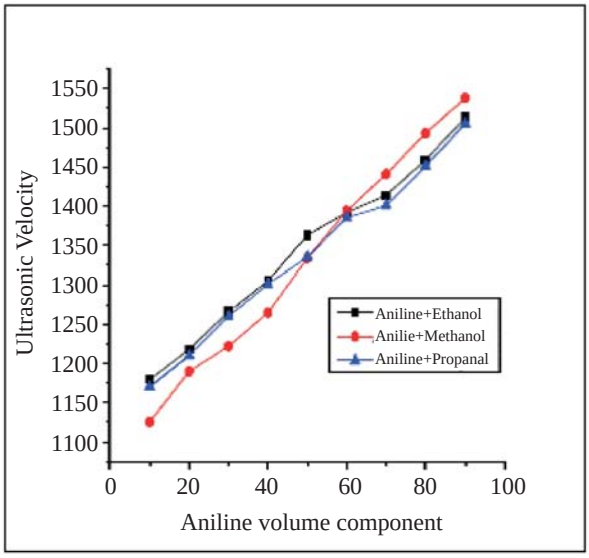

Fig. 1—Aniline volume component vs ultrasonic velocity

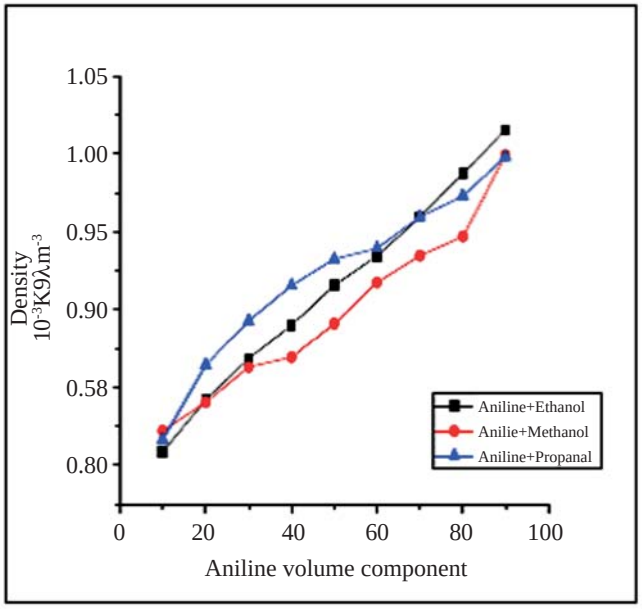

Fig. 2—Aniline volume component vs density

appearing much less reactive than Ethanol.

The density values increase with chain length of alcohols. This is in tune with[9] of the reference stating that as the concentration of alcohol increases the density also increases. Figure 2 shows variation of density of alcohols and is in good agreement with the theory postulated by Rajagopalan[10-15]. The Adiabatic compressibility (β) is calculated using the formula

$$\beta_s \rho^2 = 1/v$$

The Adiabatic compressibility (β_s) depends on the interaction between the molecules, since work has to be done against the repulsive forces between the molecules during the compression of the liquids. The decrease in adiabatic compressibility (Fig. 3) may be due to the fact that in solution the ions are surrounded by a layer of solvent molecules firmly bound to and oriented towards the ions.

The orientation of the solvent molecules around the ions may be due to the influence of the electro static field of the ions and results in an internal pressure and in a lowering of adiabatic compressibility of the solution.ie. solution becomes much harder to compress which is in tune with Sathi Reddy et al. The refractive index (n) decrease with increase in alcohol concentration as seen in Fig. 4, which shows that Propanal > Ethanol > Methanol.

The macro dielectric constant (D) is calculated (Fig. 5) using the formula which is derived from Maxwell's theory of Electromagnetism.

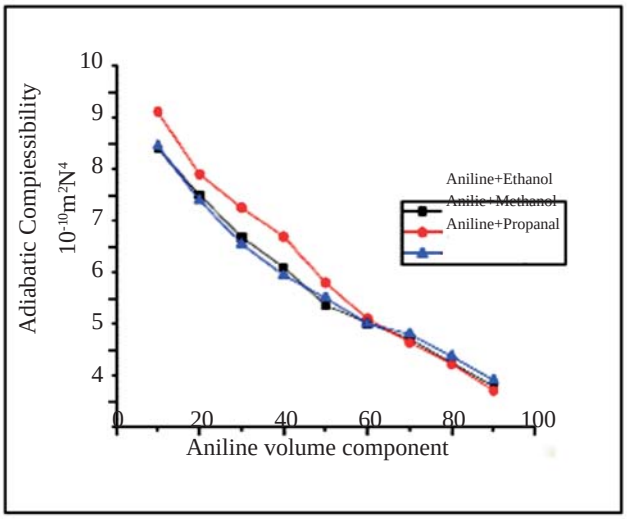

Fig. 3—Aniline Volume component vs adiabatic compressibility

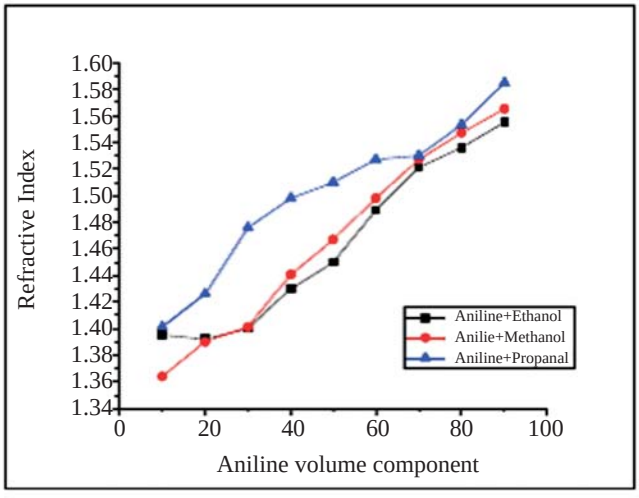

Fig. 4—Aniline volume component vs refractive index

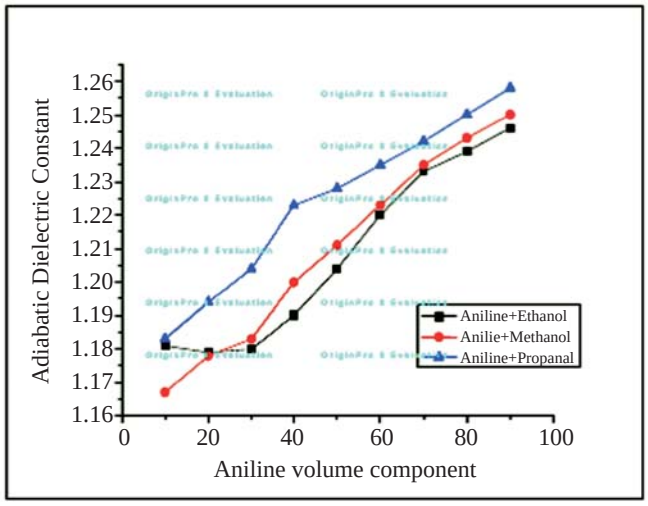

Fig. 5—Aniline volume component vs macro dielectric constant $D\sqrt{n}$

The hydroxyl group makes the alcohol molecules polar. The hydrogen bonding in alcohols makes alcohols as solvents. Alcohols are miscible in aniline because of donating nature of H + ions. A correlation of ultrasonic velocity (v) with dielectric constant indicates that there is an decrease in dielectric constant with increase in ultrasonic velocity (v). The more polar is the medium larger is the ultrasonic velocity and hence dielectric constant is larger.

Conclusion

Thermodynamical and optical studies are carried out apart from ultrasonic studies on Methanol, Ethanol and Propanol with Aniline over entire volume component percentage range. It is found that Ultrasonic velocity increases with chain length of Alcohols. Refractive index and hence adiabatic compressibility decreases with increase in concentration of alcohols..

References

1 Nomoto O. *et al*, Molecular sound velocity and molecular compressibility of liquid mixtures, *J. Phy. Soc. Japan*, 8 (1953).
2 Nath J. and Dixi A. P., Ultrasonic velocity and adiabatic compressibilities for binary liquid mixtures of Acetone with Benzene, Toulene, p-Xylene and mesitylene at 308.15K, *J. Chem. Eng data*, 29 (1984).
3 Sathi Reddy K. and Linga Reddy D., J. Acta Ciencia Indica, Acoustical and thermodynamic studies of binary mixtures of Aniline in different alcohols at 300.15 K temperature.
4 Ranganayakulu S. V., Sreenivas Reddy C. and Linga Reddy D., Ultrasonic studies of binary mixture of Ethyl Acetate and Cresols, *J. Mat. Chem. Phy*., 90 (2005) 213.
5 Ravinder Reddy B. and Linga Reddy D., Ultrasonic measurements in Etyl Acetate and n-Butanol, *Ind. J. Pure and Appl. Phy*., 37 (1999) 56.
6 Jaya Kumar N., Karunanidhi and Appan V., Ultrasonic studies of molecular interaction on binary liquid mixtures, *Ind. J. Pure and Appl. Phy*., 34 (1999) 76.
7 Ranganayakulu S. V., Sreenivas Reddy C. and Linga Reddy D., Ultrasonic studies of binary mixture of Ethyl Acetate and O-Cresol, m-Cresol, p-Cresol, *J. Acoustical Society of India*, 31 (2003) 295.
8 Prakash S., Ichhaporia F. M. and Pandey J. D., *J. Phy. Chem.*, 58 (1964) 3078. R.Turell, C. Elbaum and B. Chick, Ultrasonic methods in solid state physics.
9 Academic Press, New York and London (1969).
10 Mehrotra K. N. and Chauhan M., *J. Acustica* (1993).
11 Rajagopalan S., Free Volume and Internal Pressure Studies in Aqueous Methanol Mixtures at different temperatures, *Acoustica*, 66 (1988) 63.
12 Eyring H. and Kincaid J. F., *J. Chem, Phy.*, 6 (1983) 67.
13 Reddy K. S. and Naidu P. R., *J. Chem. Liq.*, 15 (1985) 147.
14 Bachem C., *Z. Physik*, 101 (1936) 565.
15 Reddy G. V. and Singh R.P., *Acoustica*, 23 (1970) 31.

Nondestructive evaluations of nanostructured materials

(Ph.D. thesis awarded to Dr. S.K. Verma by Allahabad University 2012)

The major findings of the research work are being given as following:

The simple interaction potential model for the calculation of temperature dependent second and third order elastic constants is validated for the nanowires of different diameters. Theoretical approach for the determination of ultrasonic attenuation in NWs at 300K with different diameters is established. There is strong correlation between size dependent ultrasonic attenuation and size dependent thermal conductivity of the nanowires. Thus an ultrasonic attenuation mechanism is established as to extract the important information about the microstructural phenomena like phonon-phonon interaction in the NWs and thermal conductivity behavior with respect to diameters of NWs at 300K.

Ultrasonic and nonlinear elastic properties of the NWs are well correlated with the stability of the NWs structure.

The predominant causes of ultrasonic attenuation in SWCNTs based materials are phonon-phonon interaction mechanism (Akhieser type loss) and thermoelastic relaxation at the room temperature.

The interaction potential model with slightly different approach is validated for the calculation of nonlinear elastic constants of SWCNTs based materials.

There is strong correlation between the length dependent ultrasonic attenuation in the SWCNTs and the length dependent thermal conductivity of the SWCNTs.

We have successfully synthesized Cu-PVP nanofluids having different concentrations of Cu metal nanoparticles in ambient condition.

The UV-Visible spectra, XRD, TEM image and SAED pattern confirm the formation of crystalline Cu-nanoparticles dispersed in PVP and also UV-Visible results are consistent with TEM results.

The Brownian motion of the Cu-nanoparticles in nanofluids produces convection like effects at the nanoscale and responsible for enhancement of thermal conductivity of PVP due to Cu-nanoparticles suspension.

On the basis of the behaviour of ultrasonic wave propagation we have developed the ultrasonic mechanism to predict enhanced thermal conductivity due to suspension of the metallic nanoparticles with very low concentration into polymeric fluid.

We have successfully synthesized Cu/Pd nanoparticles in aqueous solution in ambient condition with the addition of a complexing agent, trisodium citrate.

These Cu/Pd nanoparticles synthesized with complexing agent were suggested to have stable suspension lasting a long period of time.

The ultrasonic spectroscopic method is well established for the determination of the size of the bimetallic alloyed nanoparticles and their distribution in polymeric fluid.

Dr. Satyendra Kumar Verma
Department of Physics
Government Polytechnic
Gonda (UP) India

Information for authors

1. Type of Contribution

JOURNAL OF PURE AND APPLIED ULTRASONICS welcomes original research papers and articles related to the subject of ultrasonics. The contributions may be in the areas of physical ultrasonics, medical ultrasonics, ultrasonic non-destructive evaluation including NDT, high power ultrasonics, underwater acoustics, ultrasonic transducers, transduer materials & devices and any other related topic. These may fall into one of the following categories.

Research Papers - These should be an original research work contributing to scientific developments. They should be written with a wide readership in mind and should emphasize the significance of the work.

Reviews Articles - Includes critical reviews and survey articles.

Research and Technical Notes - These should be short descriptions of new techniques, applications, instruments and components,

Letters to the Editor - Letters will be published on points arising out of published articles and papers and on questions of opinion.

Miscellaneous - Miscellaneous contributions such as conference reports, Ph. D. thesis reviews and news items are also accepted. Recommended lengths of contributions are: Research papers 2000-4000 words, revies articles 2000-5000 words conference reports 500-1500 wordes; news items, research and technical notes up to 1000 words.

2. Manuscripts

Manuscripts should be typed on one side of the paper in double spacing with wide margins on A4 size paper. The originals of text and illustrations should bnee provided to facilitate the process of reviewing. A soft copy of the manuscript in MS WORD for text and MS EXCEL for illustrations and a PDF file thereof may be sent along with the manuscript.

Title - Titles should be short and indicate the nature of the contribution. About 5 keywords may be given after the abstract.

Abstract - An abstract of 100-200 words should be provided on the contribution. About 5 keywords may be given after the abstract.

Mathematics - Mathematical expressions should be arranged to occupy the minimum number of lines consistent with clarity e.g., $(x^2+y^2)/(x-y)^{1/2}$.

References - References should be indicated in the text by its number only. The reference number should be given as superscript. The corresponding reference shall contain the following information in order; names and initials of author(s)in bold, full title of the work, journal or book title in italic, volume number in bold, the year of publication in brackets and the page number. As example: Vasanth B.K., Palanichamy P., Jayakumar T. and Sankar B.N., Assessment of residual stresses in a carbon steel weld pad using critically refracted longitudinal (L_{CR}) waves, *J. Pure Appl. Ultrason*., 28 (2006) 66-72.

Units and Abbreviations - Authors should use SI units wherever possible.

3. Reprints

One copy of the issue in which the paper is published is sent to the author free of charges.

R.N. 39355/81

INTERNATIONAL SYMPOSIUM ON ULTRASONICS (ISU-2015)

(Theme: Ultrasound in Biomedical and Industrial Applications)

22-24 January 2015

In commemoration of

Golden Jubilee of Department of Physics,

Silver Jubilee of Department of Electronics

&

40th Anniversary of Ultrasonics Society of India

Organized by

Department of Physics & Electronics,

Rashtrasant Tukadoji Maharaj Nagpur University, Nagpur

&

Ultrasonics Society of India

Venue:

BSNL Regional Telecom Training Centre,

Seminary Hills, Near TV Tower,

Bhaskar Bhawan, Nagpur- 440 006, India

www.nagpuruniversity.org ; www.ultrasonicsindia.org

For more information, please contact -

Dr. Omprakash P. Chimankar
Convener
Organizing Committee (ISU-2015)
+91 9766969894, +91 0712-2041093
opchimankar28@gmail.com
omprakash_chim@yahoo.co.in

Prof. Vilas A.Tabhane
Chairman
Organizing Committee (ISU-2015)
Department of Physics
University of Pune, Pune-411 007
+91-20-25692678, Ext. - 301
+91-9975935358
vtabhane@physics.unipune.ac.in

Printed at Alpha Printers, BG 2/38C, Paschim Vihar, New Delhi-110063